International Journal of Disaster Risk Reduction 73 (2022) 102894

Contents lists available at ScienceDirect

International Journal of Disaster Risk Reduction

journal homepage: www.elsevier.com/locate/ijdrr

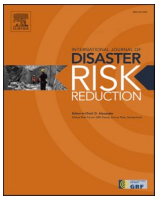

High spatial-resolution loss estimation using dense array strong-motion near-fault records. Case study for Hveragerði and the M_w6.3 Ölfus earthquake, South Iceland

Atefe Darzi [a,*], Bjarni Bessason [a], Benedikt Halldorsson [b,c], Sergio Molina [d,e], Alireza Kharazian [d], Mojtaba Moosapoor [a]

[a] Faculty of Civil and Environmental Engineering, School of Engineering and Natural Sciences, University of Iceland, Reykjavik, Iceland
[b] Faculty of Civil and Environmental Engineering, and Earthquake Engineering Research Centre, School of Engineering and Natural Sciences, University of Iceland, Reykjavik, Iceland
[c] Division of Processing and Research, Icelandic Meteorological Office, Reykjavik, Iceland
[d] Multidisciplinary Institute for Environmental Studies "Ramon Margalef" (IMEM), University of Alicante, Spain
[e] Dept. Applied Physics - Faculty of Sciences, University of Alicante, Spain

ARTICLE INFO

Keywords:
Loss estimation
Intensity measure variability
South Iceland
Empirical Bayesian Kriging
Geostatistical analyses
Seismic risk assessment

ABSTRACT

The most recent and costliest damaging earthquake in Iceland is the M_w6.3 29-May-2008 Ölfus earthquake to date. In particular, Hveragerði town located in the extreme near-fault region, suffered intense horizontal peak ground accelerations (PGA) of ~ 40–90%g and large amplitude and long-period near-fault pulses, recorded on a dense urban strong-motion array in the town. In this study we collated a high-spatial resolution exposure database (building-by-building) complete with actual reported losses and classified the buildings by building materials and construction year according to the code design requirements in place at the time.

We took advantage of the array data and evaluated a set of well-known ground motion intensity measures (IM), including PGA, pseudo-acceleration response spectra at short-to-long periods, Arias Intensity and Cumulative Absolute Velocity. We applied empirical Bayesian kriging geostatistical analyses to generate high-resolution shakemaps and provide IM estimates for each building. The shakemaps showed a significant and systematic variation of the IMs across the small study area, with the lowest ground motions observed centrally and highest values in the outskirts. Furthermore, correlation analysis was carried out for the damage ratio and the exposure data IMs, but only low-to-moderate correlations were observed. A key reason is the incurred losses were primarily due to damage to non-structural components, to which the code design requirements do not apply. We carried out a seismic loss assessment in Hveragerði for the earthquake scenario of the Ölfus earthquake both on building-by-building, and municipality levels of spatial resolution. We applied both local and global fragility models associated with detail building typologies identified based on the SERA taxonomy scheme.

The results show that the global fragility functions severely underestimate the seismic performance of the building stock, except for one-story reinforced concrete buildings, while overall the masonry buildings were associated with the most predicted and observed losses. On the other hand, the local models predicted losses that conformed well with the observed damages to timber

* Corresponding author. Faculty of Civil and Environmental Engineering, School of Engineering and Natural Sciences, University of Iceland, Hjardarhagi 2-6, IS-107, Reykjavík, Iceland.
E-mail addresses: atefe@hi.is (A. Darzi), bb@hi.is (B. Bessason), benedikt@vedur.is, skykkur@hi.is (B. Halldorsson), sergio.molina@gcloud.ua.es (S. Molina), alireza.kharazian@ua.es (A. Kharazian), mom12@hi.is (M. Moosapoor).

https://doi.org/10.1016/j.ijdrr.2022.102894
Received 13 November 2021; Received in revised form 2 March 2022; Accepted 4 March 2022
Available online 10 March 2022

and concrete buildings. The high-spatial-resolution predictions of losses gave results that better correlated with the observed losses in most typologies.

1. Introduction

Iceland is a land of natural hazards and its intense seismic and volcanic activity, driven by the localized Icelandic hotspot under central Iceland and the Mid-Atlantic Ridge, the extensional plate boundary that crosses the country. The interplay of the hotspot and the Mid-Atlantic Ridge has resulted in an eastward ridge-jump of the extensional boundary on land, constructing two major transform zones of Iceland, namely the South Iceland Seismic Zone (SISZ) and the Reykjanes Peninsula Oblique Rift (RPOR) in the southwest and the Tjörnes Fracture Zone (TFZ) in the north (see Fig. 1) [1–6]. The largest earthquakes in Iceland take place in the transform zones [8]. As a result, the seismic hazard in Iceland is highest there, with reference peak ground accelerations (PGA) having a 10% probability in 50 years of exceeding 0.5 g [7]. Moreover, the SISZ coincides with a relatively densely populated agricultural region that contains all critical infrastructures and lifelines of a modern-day society, such as towns, roads, bridges, industry, power plants (geothermal and hydropower), pipelines and electronic transmission systems.

The most recent damaging earthquake in Iceland was May 29, 2008 M_w6.3 Ölfus earthquake which struck the western part of the SISZ (Fig. 1). The earthquake occurred by the right-lateral strike-slip faulting of two parallel north-south oriented faults [8], which ruptured with a 2 s time difference [9]. The small town Hveragerði, which is the main subject of this study, was in the extreme near-fault region of the Ölfus earthquake with the epicenter being approximately 6 km away, but one of the causative faults only 1–2 km from the town (Fig. 1). As a result, the largest seismic ground motions in an urban area ever recorded in Iceland were captured on a small-aperture strong-motion array (ICEARRAY I) [10]. So far, a number of studies on the dataset have been carried out focusing on the ground motion characteristics within Hveragerði in terms of PGA and spectral characteristics [9–12] but most notably modeling their site effects [13,14] on a geology profile characterized by velocity reversals.

This worldwide unique dataset provides us an opportunity to gain an insight into the characteristics of the spatial variability of various intensity measures (IMs) in relation to the observed damage and its parametrization combined with the classification of existing structures in the region. Achieving such deep understating as one of the main goals of this study can serve as a guideline for improved and dense instrumentation as well as for optimizing urban planning strategies in urban areas in seismic regions.

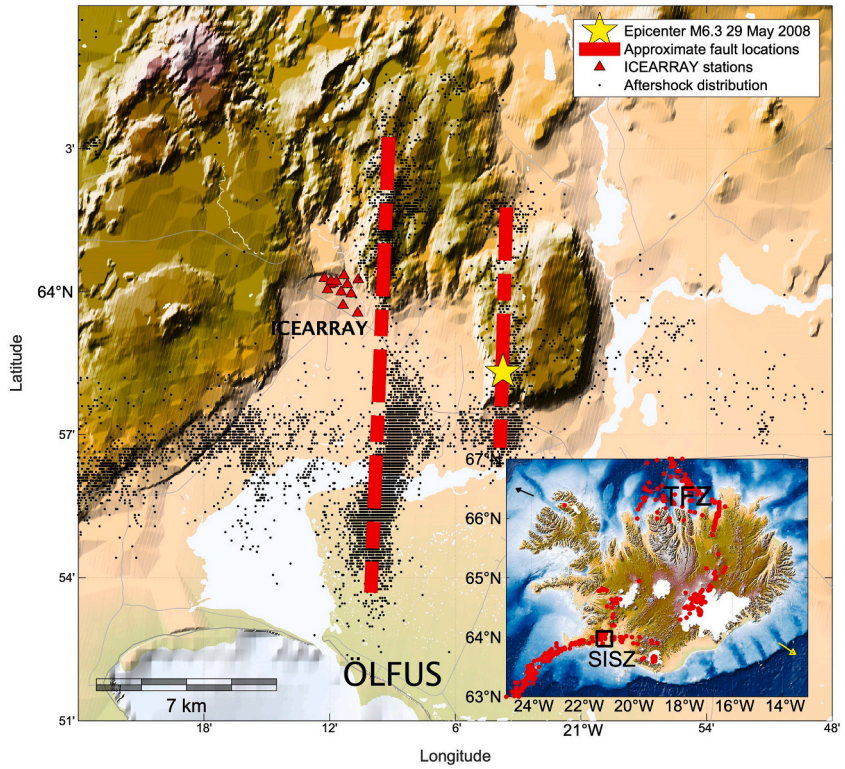

Fig. 1. The M_w 6.3 Ölfus earthquake on May 29, 2008 (yellow star denoting the epicentre) took place on two separate strike-slip faults (red dashed lines) and was followed by an intense aftershock sequence (black dots) on the causative faults and along the plate boundary. The ICEARRAY I small-aperture strong-motion array (red triangles) in the town of Hveragerði was in the extreme near-fault region and suffered the intense strong-motion. The small map shows a map of Iceland and the spatial distribution of instrumentally recorded significant earthquakes of M_w 3.1–7.1 from 1904–2019 [31] (red dots) that outline the plate margin. The seismic transform zones of the South Iceland Seismic Zone (SISZ) and the Tjörnes Fracture Zone (TFZ) are indicated.

It is well-established that modeling the spatial correlation of ground motion parameters across a region, and its corresponding effect on building portfolios have been oversimplified within probabilistic seismic loss estimation resulting in unrealistic loss estimates [15,16]. For instance, Weatherill et al. [15] demonstrated that the inclusion of spatial cross-correlation of IMs into the seismic risk analysis may often result in larger (and in certain cases smaller) losses for a portfolio distributed over a typical city scale, when compared against simulations in which spatial correlation is neglected. In recent years, several studies have developed spatial correlation models to describe the correlation between various ground motion parameters across sites separated over a distance. To do this, the empirical ground-motion prediction models are considered together with their corresponding intra-event spatial correlation models used quite often in the literature [15–20]. For instance, conditional Gaussian random ground motion fields have been exploited for portfolio loss assessment ([16,21]) as well as empirical fragility curve development [20].

In our study area, the lagged coherency matrices of the ICEARRAY I recordings conclusively show that above 2 Hz frequency, and beyond 100 m interstation distances, there is effectively no correlation between the recordings [12]. This obviates the need for spatial correlation models, in particular for high frequencies, besides, to the best of the author's knowledge, there is no well-established spatial correlation model that was explicitly calibrated to the residuals of the most appropriate ground-motion models developed for the study region in southwest Iceland.

Thus, alternatively, several international studies tackle the estimation of the spatial distribution of ground motion parameters over a target region using a specific set of observation points [22–26]. To deliver accurate prediction of ground shaking at desired locations along with explicit consideration of the incorporated uncertainties, some studies incorporate geostatistical approaches based on available recorded ground motions at various recordings stations to predict ground shaking at the neighboring locations (e.g., adjacent buildings). The kriging geostatistical method is a widespread technique used for spatial interpolation, considering spatial variability. For modeling the empirical semivariogram from the data, a Gaussian mathematical function can be used. We also acknowledge the use of general Gaussian process regressions in other modules of a risk model, specifically to explicitly consider building-to-building variability in seismic fragility assessment of building portfolios [27]. Hsieh et al. (2013) generated ground shaking maps based on 444 free-field ground motion recordings of the Chi-Chi Taiwan earthquake using Kriging interpolation method [28]. In Costanzo [25], two geostatistical techniques of the Kriging have been benchmarked and tested on earthquakes of 2016–2017 central Italy to derive shakemaps for cumulative absolute velocity (CAV) and Arias intensity (AI) parameters. In Iceland, Rupakhety et al. [29] studied the effect of variability of macroseismic intensity (MMI) in Hveragerði after the Ölfus earthquake and demonstrated difficulties in modelling geographical variability and uncertainties in MMIs. They simulated damage for a macroseismic hazard scenario corresponding to the Ölfus earthquake using ATC-13 (1985) vulnerability models and buildings vulnerability defined in terms of damage probability matrices derived from June 2000 earthquake damage data [30]. They found that ATC-13 vulnerability models should be used with caution in Iceland because although they seem suitable for Icelandic buildings undergoing relatively small levels of damage, their efficacy for larger levels of damage is not guaranteed.

Insurance against damages caused by natural hazards is obligatory for all buildings in Iceland. Therefore, in the aftermath of destructive earthquakes repair cost for all damaged buildings is assessed to fulfill insurance claims. Besides, NCI owns a fully probabilistic bespoke model for Icelandic earthquake risk assessment and a quick response deterministic model that can compute the insurance risk routinely [32]. However, the models, detail of the required assumptions and information as well as the corresponding results are not shared publicly. Despite this, to reach the main goal of this study, i.e., detailed earthquake loss prediction for a scenario event corresponding to the damaging 2008 Ölfus earthquake across Hveragerði town, this study uses an open flexible risk assessment tool [33] through which any modification can be easily implemented, and the results can be regenerated by users.

Moreover, in Iceland, all properties are registered in a detailed official inventory database by Registers Iceland (www.skra.is), which allows the construction of detailed exposure models for risk assessments. Furthermore, insurance losses can be combined with the property database to construct a comprehensive loss dataset with detailed information on each damaged and undamaged property. In this regard after the Ölfus earthquake, we establish a local detailed GIS-based building-by-building loss database for all residential buildings in Hveragerði. A dwelling-to-dwelling loss database also exists for all residential buildings affected area by the Ölfus earthquake, which has been used in several studies. It should be highlighted that it is rare in post-earthquake studies to have both access to a complete detailed loss database on building-by-building level, as well as access to recorded near-fault, high-quality waveform data with high spatial resolution for the same event and same area, in particular of such high-intensity ground motions as in the case for the Ölfus 2008 earthquake and the town of Hveragerði.

In this study, for the first time, a detailed "microseismic" loss estimation is carried out for Hveragerði and the Ölfus earthquake in South Iceland, in the sense that losses are modeled both on a high spatial resolution of building-by-building basis, as well as on municipality level, and then compared. Additionally, to gain a deep understanding of different consequences that a damaging earthquake can cause in a similar seismic-prone region, different risk metrics in terms of damage ratio, damage probability, and economic losses are analyzed. Another important advance envisaged in this study is accounting for the uncertainty of shaking IMs and building replacement value in risk analyses. Moreover, in the present study, to address the aforementioned shortcoming of using ATC-13 vulnerability models in Iceland [29], we employed the most recent local empirical fragility and vulnerability models [34], as well as global fragility models based on simplified structural models [62]. The results and predictions made by these local and global models are compared to real observed losses registered after the May 2008 Ölfus earthquake. The risk assessments are performed accounting for high spatial PGA and PSAs at short periods and with respect to detailed Icelandic building typologies that have never been considered before. These are considerable improvements with respect to the previous study and most importantly, this study helps to reduce the seismic risk by recognizing the vulnerable building classes against the similar damaging scenario.

Therefore, the main aim of this study is fourfold. First, to evaluate and map different intensity measures and their variations within the town Hveragerði based on recorded ground motion and evaluate their inter-correlations. Second, to correlate different IMs to

observed losses thus producing a benchmark for future seismic risk studies. Third, to study the influence of the seismic design provisions on the performance of the building stock within the town. Finally, to use both local and global vulnerability and fragility models in loss estimation for two levels of spatial resolutions using the Ölfus earthquake as a scenario event and compare the predicted losses with the observed losses.

2. Hveragerði and the M_w6.3 Ölfus earthquake on May 29, 2008

2.1. The ICEARRAY I dense near-field strong-motion dataset

At 15:45 UTC on May 29, 2008 a M_w6.3 earthquake took place in the Ölfus region in the western part of the SISZ, the epicenter of which was located approximately between the towns of Hveragerði and Selfoss (Fig. 1). The earthquake strong-motion in the extreme near-fault region was characterized by intense horizontal and vertical ground accelerations of a relatively short duration and large amplitude horizontal velocity pulses [9–11,35]. They were recorded on the ICEARRAY I in Hveragerði, the first permanent small-aperture urban strong-motion array in Iceland. The ICEARRAY I had been deployed in 2007 and is composed of 13 stations of inter-station distances of only 50–1900 m spread across the town [36].

Namely, the earthquake ground motion time histories revealed a complex earthquake source process [8,37] as the earthquake was found to have taken place on two parallel but separate (by ~ 4.5 km) vertical north-south striking dextral strike-slip faults with the first fault rupturing approximately 6 km from Hveragerði, with the second fault located approximately 1–2 km from Hveragerði [8] and triggered about 2 s after the first [9]. The large amplitude and long period velocity pulses observed at all ICEARRAY I stations were found to be associated with the fast and permanent coseismic ground displacements (Fig. 1) [9,38]. Along the fault parallel direction (North-South) they were associated with the surface manifestation of permanent fault displacement at depth. However, along the fault normal (East-West) component where the velocity pulse was driven by directivity effects of the approaching fault rupture front, permanent displacement was also observed. This is notable as the latter is expected to be associated with zero net displacement [e.g. Ref. [39]] and thus observed permanent displacements are due to the complex interplay between the two causative faults and the block rotation associated with the "bookshelf" tectonics of the SISZ [1,2,40–42]. The recorded ground motion amplitudes are consistent with other strong earthquakes recorded in the SISZ and their variation across the array does not appear to be greatly affected by the variable site effects reported. Still, the lagged coherency matrix of the strong-motion recorded on the ICEARRAY I when calculated for the fault-normal, fault-parallel and vertical components show that the recorded fault-normal ground motions are strongly coherent over the entire array at frequencies below 2 Hz. The same was observed for the fault-parallel component, but much less inter-component coherency between the two was found. These observations are consistent with the strong presence of the observed long-period near-fault pulses. However, at frequencies higher than 2 Hz, and for inter-station distances beyond 100 m, much less coherency was found, which in turn is manifested in the recorded variability of the peak acceleration and velocity values, and in the pseudo-acceleration response spectra [10,12].

2.2. Physics-based strong-motion parametrization

The ICEARRAY I dataset for the Ölfus earthquake forms the basis of this study. The data from 10 stations is used as two stations were not operational at the time of the earthquake, and the third is co-located with another station. Representative ground motion IMs are calculated from the three-component acceleration recordings of these stations and used as a proxy for the loss estimation that follows. Four different IMs are used that allow the parametrization of different characteristics of the ground motions. They are the PGA, the pseudo-acceleration response spectrum (PSAs) for 5% critical damping ratio over the period range of engineering interest, and two energy-based parameters, the Arias Intensity (AI) and Cumulative Absolute Velocity (CAV). PGA is commonly used to present the

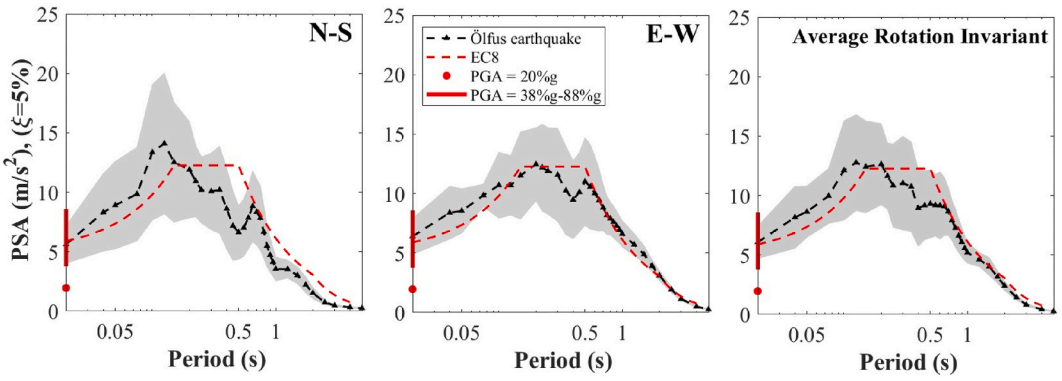

Fig. 2. Pseudo-acceleration spectral response curves plotted vs. the natural periods of a 5% damped simple oscillator calculated from the ICEARRAY I recordings of the May 29, 2008 Ölfus earthquake. The mean (black dashed line with symbols) and the extent of its standard deviation (grey area) are shown for the horizontal components (N–S, fault parallel; E-W, fault normal), along with the average rotation-invariant of the two components combined. We showcase the observed range of horizontal PGA values (38.4–87.6%g) by the vertical red line on the left *y*-axes for the specific comparison with the red dot on the y-axes that represent 20%g, which was the design acceleration for the majority of the building stock that suffered the earthquake. After the earthquake, the design requirements were updated to their present form, the elastic response spectrum for 5% damping ratio (red dashed line).

degree of severity of ground motions and to scale seismic loads in design codes. It is generally associated with the high-frequency components of an earthquake motion (Kramer, 1996) and thereby, as a proxy for the seismic damage potential for stiff structures with short natural periods. PGA, however, does not necessarily reflect how earthquake motion affects a structure. The well-known acceleration elastic response spectra depict the maximum response of elastic SDOF-systems to given ground motion. PGA and the PSAs provide peak or maximum amplitude and do not reflect the duration of a ground motion, or the number of destructive cycles of the ground motion. Other parameters, such as AI and CAV, reflect this better, as well as number of other parameters given in the literature [43].

Fig. 2 shows the PSA for all ICEARRAY I horizontal accelerograms along the N–S (PSA_x) and E-W (PSA_y) directions separately. The dashed black line depicts the mean values, and the grey shaded area displays the mean plus/minus one standard deviation (for details see Ref. [10]). For simplicity of modelling, the horizontal components of ground motion measures have been combined into one value [see in e.g. Refs. [44–47]]. In this study we use the average rotation-invariant (ARI) of the two horizontal components (PSA_{ARI}) [48] that gives the expected (mean) values of response spectra for all possible orientation of accelerometer axes in the horizontal plane. We note that the ARI measure of the Icelandic dataset of strong-motions is essentially equivalent to the geometric mean [49].

Fig. 2 shows the very large values of PSA exceeding 10 m/s^2 (~1.0 g) over short periods of 0.08–0.38 s. A great majority of the building stock in Hveragerði is stiff low-rise structural wall buildings. The natural period of concrete and masonry buildings is assumed to be ~0.1 s whilst for timber buildings it is around 0.2 s. The 77.5% of the building stock in Hveragerði was built before 2002 when no design spectrum was implicitly defined, and buildings were designed on the basis of PGA of maximum 20%g [35]. In other words, the vast majority of buildings in Hveragerði experienced much larger accelerations than the code design value specified. To illustrate this, we have marked 20%g with a red dot on the *y*-axes and contrast that with a vertical red line from 38.4%g to 87.6%g on the *y*-axes that represents the large, measured PGA amplitudes and its variation in Hveragerði during the Ölfus earthquake. For comparison with the in-force design spectrum for Hveragerði, the Eurocode 8 elastic response spectrum for 5% critical damping (soil class A, $a_{gR} = 0.5$ g) is depicted with red dashed line. It can be noted that the right corner-period, T_c, is 0.5s (not 0.4s), which is according to the National annexes to account for near-fault effects in the area [7]. It is evident that buildings constructed after the implementation of the present Eurocode are designed for seismic loads similar to the recorded loads during the 2008 Ölfus earthquakes. On the other hand, buildings constructed prior to the implementation of Icelandic National Application Documents of Eurocode 8 in 2002 were designed for much less seismic loads, by a factor of 2–4.4, and therefore suffered extremely from the Ölfus earthquake.

Most notable in Fig. 2, however, is the fact that the PSAs at $T < 0.6$ s are clearly associated with large variability compared to longer periods, even over the small spatial scale of the ICEARRAY I (~1.25 km^2). Since short-period motions are more susceptible to small-scale differences in source, path, and site effects that are not modeled (i.e., effectively considered random) the use of PSA_{ARI} serves a clear purpose at $T \leq 0.5$ s. At longer periods, however, even though the variability appears to be greatly reduced, we choose not to combine the strike-parallel (*x*, N–S) and the strike-normal (*y*, E-W) components since they exhibit different PSA characteristics due to the different physical origins of the near-fault velocity pulses along those two directions (see description above). The near-fault velocity pulse along the strike-parallel component appears in the PSA as a narrow-band increase at T ~0.7 s, associated with a permanent surface displacement along the fault, while the near-fault velocity pulse along the strike-normal associated with the propagating fault rupture towards Hveragerði, appears as a rather broad-band increase in PSA values from $T \sim$ 0.5–2 s [10]. This separation is to

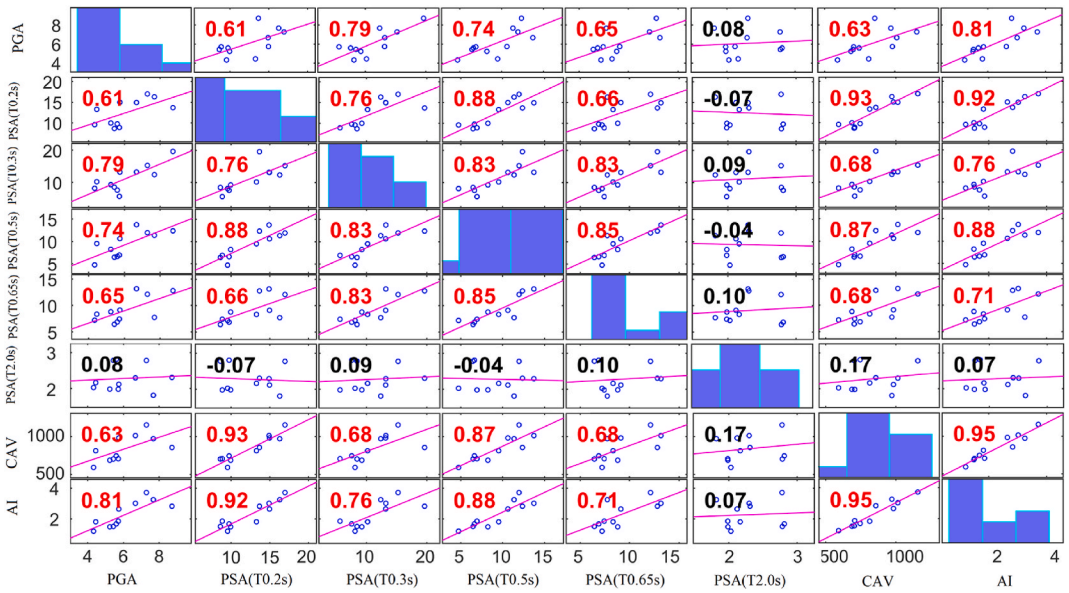

Fig. 3. Correlation matrix of a set of averaged horizontal IMs (in m/s^2) at ICEARRAY I stations. The correlation coefficient is displayed on the top left corner of each panel. Histograms of the recorded IMs are shown in the diagonal of the matrix.

facilitate a more physics-based interpretation of the spectral loading at long periods, further justified in Fig. 2c where the PSA_{ARI} is shown at all frequencies, showing clearly that it masks completely these near-fault effects at longer periods.

It is informative to study the correlation between the selected IMs because depending on their dynamic structural properties different elements of the exposed infrastructure respond differently to the seismic ground motions. For this purpose, a correlation matrix for the seven IMs is shown in Fig. 3 based on the IM-values of each station calculated from the recordings. Histograms of the IMs over their ranges appear along the matrix diagonal with scatter plots of IM pairs on the off-diagonal. To present the general trend of the IMs correlation, a least-square analysis is conducted for each set of IM datapoints. The slopes of the least-squares reference lines in the scatter plots (pink lines) are equal to the displayed correlation coefficients shown in the panels. As can be seen in subfigures of Fig. 3, there is a positive slope for almost all IMs, except for PSA at T 2 s. The p-values and number of degrees, that is nine (11-2 = 9), are used to test the hypothesis that there is no correlation between the observed phenomena (null hypothesis). Based on the t-statistic, an off-diagonal element of p-value must be less than the 0.05 significance level, to indicate a significant correlation between the two IMs in

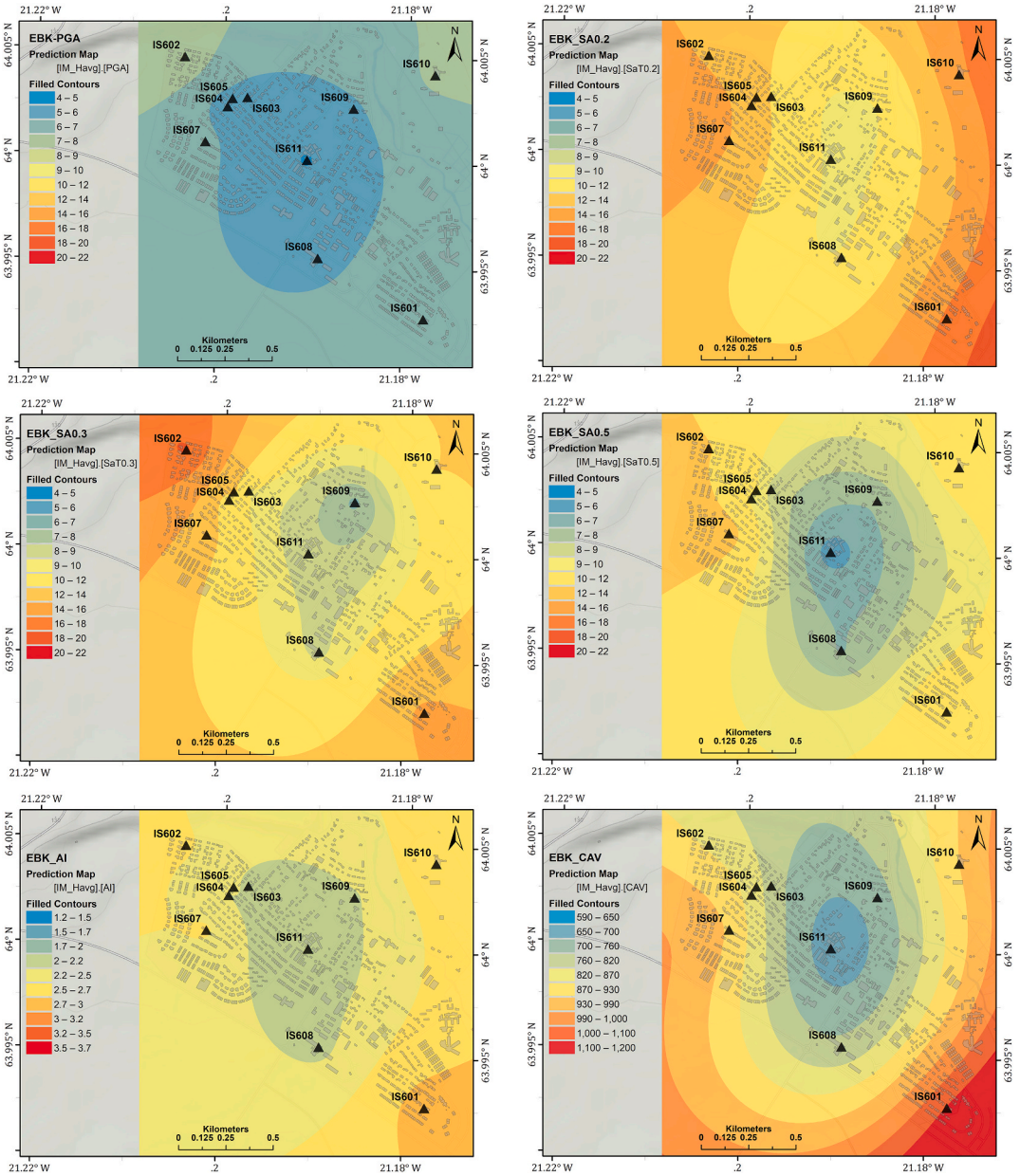

Fig. 4a. Shakemaps illustrating the spatial distribution of rotation invariant component of horizontal motions represented by the IMs PGA, and PSA_{ARI} at oscillator periods T of 0.2, 0.3, and 0.5 s (from top left to middle right) across Hveragerði relative to a single discretization of the amplitudes in m/s^2. At the bottom are the shakemaps for the IMs AI (left) in m/s and CAV (right) in cm/s. The Empirical Bayesian Kriging (EBK) geostatistical analysis is applied to interpolate the IMs across Hveragerði on the basis of the ICEARRAY I recordings (triangles) with buildings indicated by light grey polygons.

question. To reflect this in Fig. 3, the Pearson correlation coefficient is displayed in red if p-value < 0.05, otherwise it is shown in black color. The p-value was much less than 1% in the vast majority of the cases shown, but some ranged from 2 to 4%.

The IMs from PGA down to PSA at 2 s is essentially representing the narrow-frequency-band amplitudes of the ground motion from high-to low-frequency motions, while the CAV and AI being more involved estimates. The relatively high correlation of PGA and PSAs at adjacent and relatively close periods is therefore to be expected, as is the case for PGA down to PSA at 0.65 s. Similarly, the lack of correlation of PSA at 2 s with any of the others was expected, as long-period motions are effectively blind towards small-spatial scales, such as the overall area of the array. The highest correlations are found between the energy-based IMs CAV and AI, and then between both and PSA at 0.2 s.

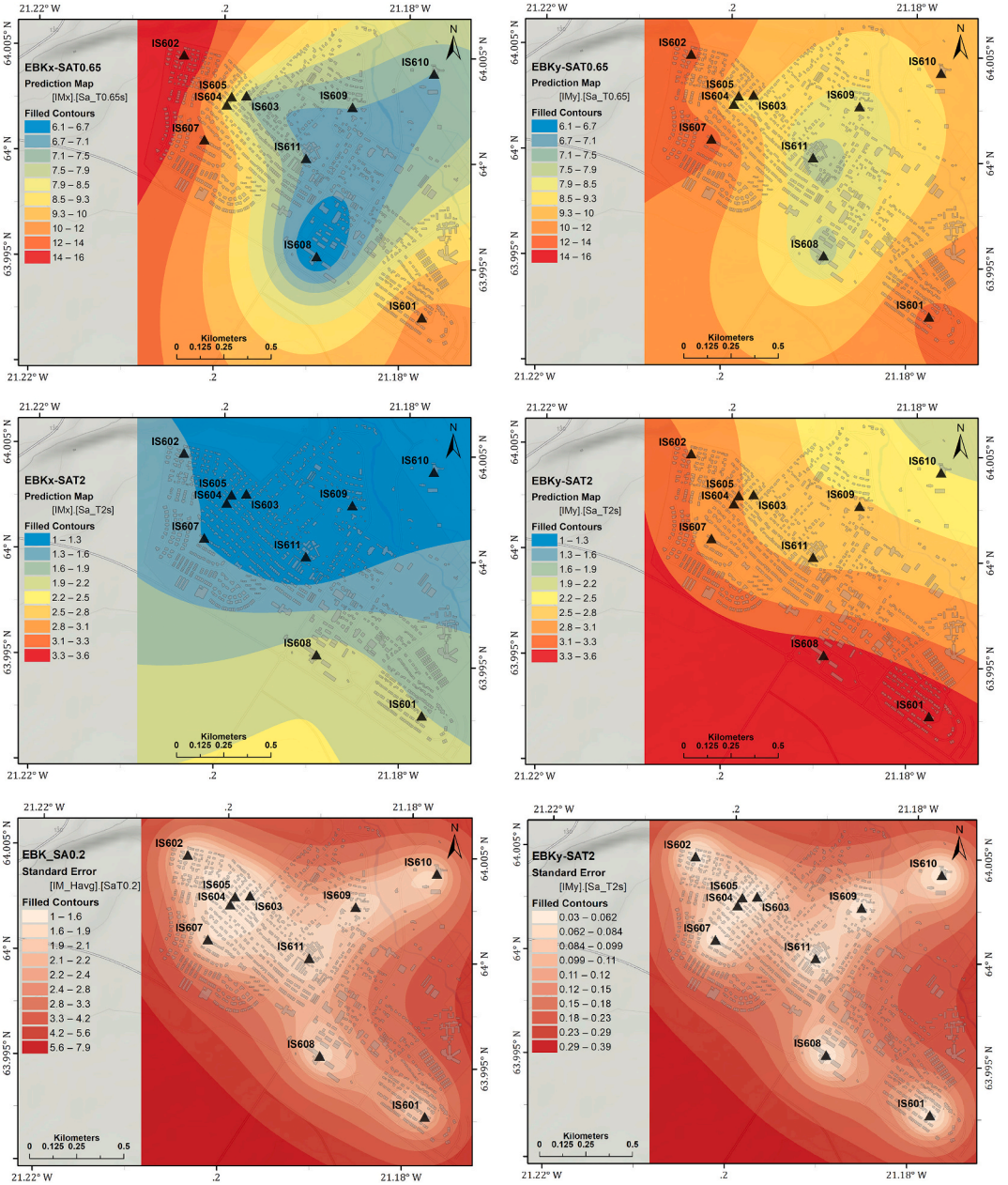

Fig. 4b. Same caption, except the shakemaps are shown for the separate horizontal components of motion along the N-S direction (left) and E-W direction (right) for PSA at $T = 0.65$ s (top), which coincides with the period of the near-fault velocity pulse associated with fault dislocation, and 2 s (middle) which shows the disparity between the fault normal (E-W) amplitudes associated with propagating rupture front. The two bottom plots show examples of the standard errors of two of the IMs estimates (0.2 and 2 s PSA at left and right, respectively). The maps highlight the spatial areas of relatively low standard errors i.e., those areas where we can expect to have full confidence in the interpolation. The opposite is observed in places outside of the array area.

2.3. High-resolution geospatial modeling of shaking variability

The observed variability of the short-period motions across the array and their high spatial recording density now provides the opportunity to construct shakemaps for a number of ground motion IMs in high spatial resolution. To model the likely ground motions at non-recording sites we use geostatistical interpolation methods to estimate the values in unsampled locations and thus project the observed data into a continuous form in raster data format. Specifically, we use spatial kriging interpolation which is one of the most frequently used interpolators that offers a minimum sampling error variance. Discrepancies and sampling errors are then evaluated in the spatial analysis using variograms. Hence, a semivariogram model measures the dissimilarity between the interpolated value and observed data. Its accurate estimation is the most difficult aspect of building a valid kriging model. To elaborate, the classical kriging method uses a single semivariogram model to make predictions at unknown locations, implicitly assuming that the estimated semivariogram is the true semivariogram for the interpolation region and thereby underestimates the standard errors of prediction. On the contrary the Empirical Bayesian Kriging (EBK) geostatistical method is a robust interpolation method since it uses hundreds of semivariogram models, which offers significant advantages such as more accurate prediction for small datasets, more accurate standard errors of prediction, and minimal interactive modelling [50]. In the EBK process, a semivariogram model is first estimated from the observed data (samples). It should be noted that in EBK, the semivariogram parameters are estimated using restricted maximum likelihood. Then, at each data site, a new value is simulated using this semivariogram. Afterward, a new semivariogram model is calculated from the simulated data. A weight is assigned to this semivariogram based on Bayes' rule indicating how likely the observed data can be generated from the semivariogram. The process is repeated for the optimal number of iterations ranging from 100 to 500, thereby resulting in numerous sets of simulated data at the input sites from which a new semivariogram model is estimated along with its corresponding weight. Using weights of the estimated semivariograms, surface predictions and their corresponding standard errors are computed at the unsampled sites across the study area.

To illustrate the spatial variability of the selected IMs, we apply the EBK spatial interpolation technique through Esri's ArcGIS Geostatistical Analyst to generate their corresponding shakemaps (prediction maps) over Hveragerði. The EBK technique predicts the value of a parameter (i.e., the IM of interest) at target locations, i.e., very small grid cells across Hveragerði. The semivariogram model type employed in this study is K-Bessel which is the most flexible and accurate model as it best characterizes the spatial autocorrelation in the data. To satisfy the stationary hypothesis when applying EBK, the trends of the input spatial data were removed initially if they exist. A valuable by-product of the EBK is the variance map which gives us a measure of uncertainty in the interpolated values as they are essential for decision-making purposes.

Fig. 4a presents the EBK-based shakemaps for PGA, short-period PSA_{ARI} at T 0.2, 0.3, and 0.5 s, as well as AI and CAV and finally for PSA_x and PSA_y at 0.65 and 2.0 s. Buildings and ICEARRAY I stations are indicated in light grey polygons and black triangles, respectively. The IM classes used for mapping the respective shakemap (see the legends) are different from each other but presenting the same color scheme so that they are internally comparable, apart from AI and CAV that have other units. The most noticeable feature of the spatial distribution of horizontal IMs in Fig. 4a is the persistently lower levels in the central part of Hveragerði, where IS608, IS611, and IS609 sites are located, while larger IMs are observed on the outskirts of town. This pattern was consistently seen for IMs for peak parameters at short and intermediate periods but not at long periods.

The consistent color scheme shows that the spatial variation of horizontal PGA appears to be considerable, having a minimum between 4.3 and 5.2 m/s^2 and a maximum of 7.3–8.7 m/s^2. Nevertheless, this variability is rather small compared to that of PSA at short periods. This relative increase in variability is also manifested in Fig. 2, but Fig. 4b has the advantage of revealing also the spatial pattern with the lowest ground motion IMs generally observed in the center of Hveragerði with highest values at the outskirts. The other IMs, the AI and CAV also reveal this pattern, but in different ways, as they appear to capture the salient features of all PGA and low-period PSAs i.e., those associated with high-frequencies, and in particular the PSA at 0.2 s, consistent with the correlations between the estimates as presented in Fig. 3. They, on the other hand, reflect very little the different characteristics of the intermediate (0.65 s) and long-period (2 s) PSA maps.

Namely, the separate components of horizontal PSA at 0.65 s and 2 s are not similar to one another. The PSA_x at 0.65 s, which coincides with the narrow-band velocity pulse along the North-South component that originates due to the extreme near-fault surface manifestation of the fault dislocation at depth (see also Fig. 2), appears to show the same pattern of low values in the center of town. However, the East-West component however is associated with the velocity pulse due to rupture directivity that apparently produced sustained high levels of PSA over a broader period-range. Nevertheless, the patterns appear to be similar, indicating that the spatial effects are mapped into the velocity pulse distribution of amplitudes. The PSA at 2.0 s however, do not show a systematic pattern. In addition, they show very different levels of amplitudes, with the E-W component having much higher ones, presumably due to the broad-band nature of the forward directivity pulse. In addition, long-period waves are associated with longer wavelengths and therefore relatively low variability of the ground motions is expected over small distances, as appears to be the case here, and in particular compared to the high-frequency IMs.

Finally, we show two maps that show the spatial distribution of the standard deviations of the 0.2 and 2 s PSA interpolated values across the array. Effectively, through the relatively low values of standard deviation over the map (dark colors are higher, lighter colors are lower level) we can identify the areas where we have full confidence in the EBK interpolation. Namely, the lowest values (highest confidence) are observed in the vicinity of observations (i.e., ICEARRAY I stations), while at locations far from the nearest observation, larger uncertainties are observed and thereby less confidence. Not surprisingly, we cannot associate any confidence in the empirical interpolation values outside of the ICEARRAY I area, as reflected in the very large uncertainty values.

The clue as to why the central part of the town exhibits lower motions may be found in the town's geology. A historical earthquake N–S fault has been mapped and lies directly through the center of town (west of IS609, under IS611 and IS608 stations, and further

south). Furthermore, the fault serves as a conduit for geothermal water that reaches the surface, resulting in a geothermal area in the center of town and a widespread and elevated ground temperature gradient around IS611 and towards the north [51]. Then, underneath the surficial lava layer of several meters is a softer sedimentary layer, resulting not only in a velocity reversal, but has been affected by the geothermal activity [52]. Therefore, this elongated area is believed to attenuate higher-frequency motions more effectively than the outskirts of town, where this effect is not observed in local geology, and not in the strong-motion data. These spatial differences in geology are also what is believed to contribute to the large scatter in the observed high-frequency motions. Eventually, we notice that at longer periods, the size of the small-aperture array becomes comparable in size or even small compared to the seismic wavelengths, and such small-spatial scale effects are less systematically observed.

3. High spatial-resolution loss database for Hveragerði

3.1. Exposure database and code classification

In this study, a comprehensive exposure database was compiled for all dwellings in Hveragerði importing data from the official property database (Registers, 2019). The database stores key information such as construction year, type of occupancy, construction material, number of storeys, geographical coordinates, floor area, lateral load resisting system (LLRS), lateral force coefficient, etc. It also contains results of valuation for taxation and replacement value (reconstruction insurance value). First, dwelling characteristics are aggregated to construct a building-by-building exposure database. Then, it is collocated with the Open Street Map buildings through validation and integration in ArcGIS for clear spatial visualization.

The official property database does not include information on the structural system nor the lateral force coefficients used in seismic design. In Iceland, structural walls dominate LLRS in almost all buildings, regardless of the construction material or typologies. This contradicts other regions such as southern Europe, where moment-frames with or without masonry/brick infills are commonly used for constructing residential buildings. In this study the lateral force coefficient (defined as the fraction of the weight of the building) for RC buildings are estimated based on the buildings' construction year and the seismic design codes that were in practice for constructing buildings in different periods in Iceland (Table 1) (See also [46]). There were no seismic design codes used before 1958, marked as CDN in the code classification column in Table 1. In 1958, the first hazard map for Iceland was published in the Icelandic Journal for Engineers [54]. Although no seismic code nor regulations were operative at that time, the map affected the seismic design and most engineers started applying static lateral seismic force in their structural analysis, the low code period started (CDL). The first seismic code (ÍST 13) was then implemented in Iceland in 1976 [55]. In 1989, the seismic code was upgraded and in force up to 2002 [56]. However, there was only minor increase in the lateral force coefficient (Table 1) and the period from 1976 to 2002 can be combined into the moderate code period (CDM). Then, in 2002, the high code (CDH) period began when the Eurocode 8 and the corresponding National Application Documents were implemented [47] and there was a considerable increase in lateral force coefficient defined by design spectrum (Table 1). An updated version then came in 2010 with National Annexes [7]. It can be assumed that the moderate ductility class (CDM) has most frequently been used for the seismic design of the low-rise Icelandic in the high seismicity zones since 2002. This is the same conclusion as in Crowley et al. [53] for the European building stock after implementation of Eurocode 8. In more detail, the assumptions made for determining the lateral force coefficients in Table 1 after 2002 is that the low-rise RC buildings in Iceland have short fundamental period of vibration and therefore the flat part of the design spectrum can be used, soil class A (rock with $S = 1.0$) is assumed. Furthermore, CDM and uncoupled structural walls are assumed which results in a behavior factor of q = 3, and finally, the importance factor $\gamma_I = 1.0$ is used. The reference acceleration $a_{gR} = 0.4$ g is used for the 2002–2010 period and $a_{gR} = 0.5$ g after 2010 [7,57].

In Fig. 5, the geographical distribution of residential buildings constructed prior to the Ölfus earthquake in Hveragerði is plotted relative to the ICEARRAY I stations (black triangles) and color-coded by construction material (Fig. 5a) and construction year (Fig. 5b). In Fig. 5b the color-coding is consistent with Table 1 so that buildings built according to the same design requirement are shown in the same color and the corresponding lateral force coefficient is reported in parentheses in the legend. The color scheme from dark red to green indicates stronger design requirements i.e., higher to lower seismic vulnerability. As is generally the case, the oldest buildings, both CDN and CDL, are located in the middle of the town. In fact, the vast majority of the buildings in Hveragerði that suffered the Ölfus earthquake were built during either no, low or moderate code periods i.e., the relative percentages (number) of buildings associated with the four code classifications CDN to CDH in Table 1 are 12.2% (92), 33.9% (257), 31.3% (237) and 22.6% (171), respectively. Then, the main construction material 55.6% (421 number), 38% (288), and 6.4% (48) of the residential building are reinforced concrete (RC), timber (wood), and masonry material, respectively, with no masonry structures constructed during CDH. Among the residential buildings in the study area, 92.2% are low-rise single-family townhouses, and the remaining comprises apartment buildings, garages, and vacation resorts. Moreover, 85.5%, 13.7%, and 0.8% of buildings are one-storey, two-storey, and three-storey (the tallest) buildings, respectively. The maximum number of storeys for masonry buildings is two, and the two oldest masonry buildings were constructed in 1935 and 1940 in Hveragerði.

It is interesting to note that in an international context, the Icelandic building stock is relatively young. For instance, in the whole of Iceland, no building was constructed before 1870 [58], and the oldest building in use in Hveragerði is a timber building from 1929. Most Icelandic RC buildings are in-situ cast, and only a few are built by prefabricated elements. The masonry buildings were constructed of unreinforced manufactured hollow pumice blocks in walls and tied together with rigid reinforced concrete floors. The pumice is a volcanic rock with high porosity and very low density (<10 kN/m^3). The weight density of the cast hollow pumice blocks is $\sim$14 kN/m^3, which is low density compared to the density of common natural stone or clay brick masonry building material in south-Europe. This results in lower inertia forces in Iceland [58].

Table 1
Lateral force coefficient used in design of RC buildings located in the zones with the highest seismic hazard in Iceland. See also Crowley et al. [53].

Construction period	Lateral force coefficient	Design code	Code classification
<1958	–	No code	CDN
1958–1976	0.07-0.1	Only hazard map (Tryggvason et al., 1958) [54]	CDL
1976–1989	0.13	Seismic code ÍST 13 (Iðnþróunarstofnun Íslands, 1976) [55]	CDM
1989–2002	0.16	seismic code ÍST 13 (Iðntæknistofnun Íslands, 1989) [56]	
2002–2010	0.33	Eurocode 8 and National Application Documents (Staðlaráð Íslands, 2002) [57]	CDH
>2010	0.42	Eurocode 8 and Icelandic National Annexes (Staðlaráð Íslands, 2010) [7]	

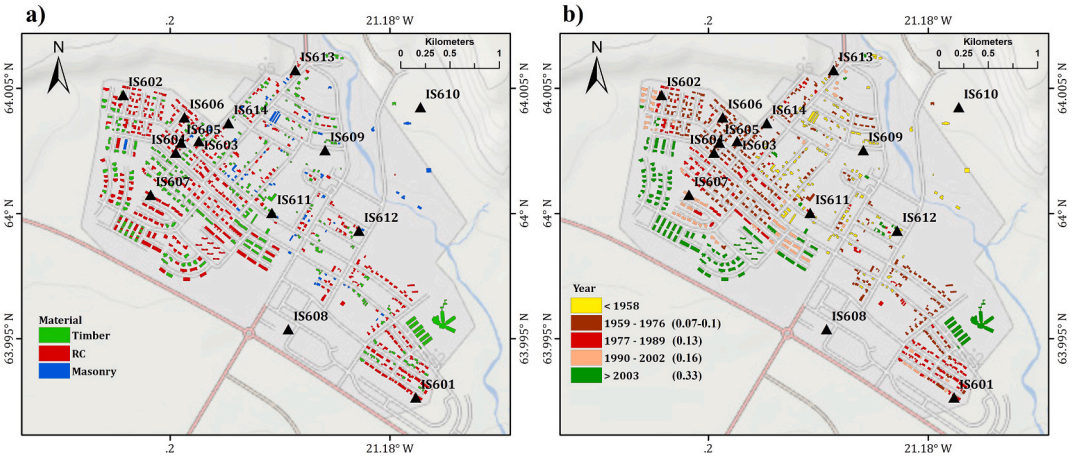

Fig. 5. Spatial distribution of buildings in Hveragerði over its respective street map classified by (a) construction material and (b) year of construction along with the corresponding lateral force coefficient (in g) reported in parentheses in the legend. ICEARRAY I stations are plotted by black triangles.

3.2. Loss parametrization

All dwellings in Iceland have compulsory catastrophe insurance provided by the Natural Catastrophe Insurance of Iceland (NCI) which has public ownership (www.nti.is). In 2008 the deductibles where ~500 Euros for each dwelling. This amount has now been raised to ~2700 Euros. In the aftermath of the 2008 Ölfus earthquake, trained assessors working for NCI estimated the repair cost for all dwellings whose owners issued insurance claims. Due to the low deductible at that time, it can be assumed that all damages were reported as it financially benefits the owners to file a claim. If no claim was filed, the building is assigned "No damage" in the loss database. Therefore, detailed empirical loss data was established for all dwellings in the affected area, including damaged and undamaged dwellings. The damage records of dwellings constituting one building are combined, thereby determining each building's damage value. Afterward, we attach the building damage information to the replacement price of each building from the exposure database described in the previous section. The replacement value in the property database is calculated by depreciated replacement value estimated based on the material, age, and general condition of the building with the addition of the cost of removing the damaged property.

The repair cost for each unit was categorized into subgroups of structural and non-structural losses (see Ref. [59]). In Hveragerði, the ratio of non-structural damage to overall damage was above 80% for RC and timber buildings, and around 65% for masonry buildings due to the Ölfus earthquake. In this work, however, the emphasis is on the aggregate total loss value for each building which is presented by the damage ratio (denoted as DR hereafter). DR is the ratio of estimated repair cost to the replacement value of each building. The DR is bounded to be in the range [0,1], where 0 refers to the no-loss and 1 (100%) indicates a total loss. Approximately 5000 residential buildings were affected by Ölfus earthquake [59]. Of those, 757 were in Hveragerði, where the most significant earthquake action was observed. Fortunately, however, the Ölfus earthquake did not cause any collapses of residential buildings but extensive damage was nevertheless observed, mainly dominated by damage of non-structural elements such as flooring and partition walls [35,59]. For instance, two buildings with timber and masonry material built in 1950 were utterly damaged (DR = 1) and one masonry building constructed in 1940 was severely damaged with DR greater than 60%. Of 757 residential buildings constructed prior to 2008 in Hveragerði, 20.5% (i.e., 155 buildings) were not damaged.

The total average damage ratio was 4.1% (ratio of summed repair cost to summed replacement cost) in Hveragerði during the Ölfus earthquake. It should be noticed that according to the post-earthquake surveys conducted by NCI after the Ölfus earthquake, in most buildings damaged in south Iceland, a significant part of the losses was pertinent to the non-structural defects such as cracks in partition walls and ceilings, wall tiles, permanent tilt and settlement of foundations. The damage ratio above includes damage of all interior fixtures, pluming, etc. but does not include damage to household items, TVs, PCs although these articles were in many cases damaged severely.

4. Earthquake strong-motion variability, code classifications and observed losses

4.1. Correlation analysis

Observed losses in Hveragerði during the Ölfus earthquake, as in any other earthquake, are related to the ability of any given structure to withstand seismic loads as well as the earthquake action the structures are subjected. On the basis of the loss dataset for Hveragerði, we show in Table 2 the observed mean damage ratio (MDR) classified by the three main building materials used in Hveragerði as well as with respect to the status of seismic design codes as specified in Table 1. To quantify observed MDR, we calculate the mean value of the observed DRs associated with **N** number of buildings included in each group. Overall, the MDR decreases with increased requirements in the seismic code.

By taking advantage of the geospatial EBK results presented for the various IMs we can obtain the predicted IM values at each building for which we have loss data, and therefore incorporate the spatial variability of the ground motion into the comparison to losses. Thus, we pair the observed damage ratios for each building from the loss database with the IMs value at each building location according to the shakemaps. While this can be done for the different building materials and different status of seismic codes (Table 2), some grouping is required due to limits in the data and small differences in MDR between groups of different code statuses. Here, the groups for CDN and CDL are combined for the RC, timber and masonry buildings. In total there are seven building groups including only one group for the masonry buildings. Fig. 6 depicts the correlation between the inferred IMs and observed DRs corresponding to the building level for these groups. 98.3% of residential buildings experienced damage ratios less than 20% while a few numbers of buildings indicating DR>20% are dispersed amongst different groups with majority of them (10 out of 13) are found in three groups associated with CDN + CDL (see Fig. 6a, d, and 6g). Thus, to preclude the effect of outlier data in the analyses due to very few numbers of empirical loss data points with large DR, datapoints with damage ratios greater than 20% are excluded from the loss dataset.

There is a great scatter in the loss data and the correlation is poor and up to moderate as shown in Fig. 6 where DRs for each code-and-material group are plotted. Despite the grouping, the correlations are affected somewhat by the number of data points (Table 2). As expected, most data points are found for the CDN + CDL and CDM for RC buildings, then for W-CDN + CDL, W-CDM and RC-CDH, as they were the prevalent building materials during those periods.

The least number of data points is found for masonry. With that in mind, for the CDN + CDL groups regardless of the building material (Fig. 6a, d, and g), the correlation seems poor in all cases (only black values). The score appears to be “most moderate” for AI and CAV and larger than ~10%. We note however the *p*-value is slightly greater than 0.05 indicating that the hypothesis of zero correlation cannot be rejected. The RC-CDM and W-CDM groups stand out, as the DRs show consistent and moderate correlation with all IM (with the strange exception of RC-CDM and PSA at *T* 0.65 s). That indicates that the relative differences in spectral ground motion amplitudes had slight effect on the DR distribution. In between them, the W-CDM group is the one associated with the highest overall correlation values, from 0.29 to 0.41 across the IMs consider, with the largest values associated with AI and CAV. Then, the highest DR correlation for the RC buildings is for PGA. Interestingly, the W-CDH DRs have the highest correlations with PGA, while for the RC-CDH buildings the score is fair for all the IMs parameters except for PSA *T* 2 s.

A much better correlation of DRs with IMs would have been expected given the high amplitude and intense seismic ground motions that in most cases far exceeded the design provisions of the buildings. However, the poor correlation has a physical explanation. Namely, the observations of the in-situ survey of the damaged buildings conducted after the Ölfus earthquake showed that the non-structural components were the primary elements that were damaged and not the structural elements [59]. In other words, the structural elements were not the key factor in the determination of the damage ratio. Furthermore, the seismic performance of the structural elements of the primarily residential buildings in Hveragerði can be attributed to them for the largest part being low-rise one-storey single buildings with light roofs, symmetric and regular design in plan and height, as well as well-designed structural walls LLRS, which for example for the RC buildings responded in the elastic range. Their residual strength is not associated with advanced seismic design but more building traditions and environmental factors that require strong walls to deal with cold climate and to withstand strong wind loads, the wind especially affecting the design of light-weight timber buildings. Furthermore, for the CDH buildings, the participation of gravel fill foundations have most likely effectively filtered out some spectral ground motion amplitudes and thus reducing the earthquake action [29,35,60].

5. Seismic loss estimation for Hveragerði using local *vs.* global models

5.1. Taxonomy and methodology

One of the main objectives of the present study is to contrast the reported losses due to the M_w6.3 Ölfus earthquake in Hveragerði

Table 2
Number of residential buildings (N) and the mean damage ratio (MDR) for different status of seismic codes (no-code, low-code, moderate-code, and high-code), for RC, timber and masonry buildings in Hveragerði following Ölfus Earthquake.

Status of seismic codes	RC		Timber		Masonry		Total
	N	MDR (%)	N	MDR (%)	N	MDR (%)	MDR (%)
CDN	15	5.1	44	5.4	33	9.1	6.9
CDL	161	5	82	3.3	14	3.1	4.4
CDM	144	4.5	92	3.7	1	0	4.2
CDH	101	2.7	70	2.5	0	0	2.6

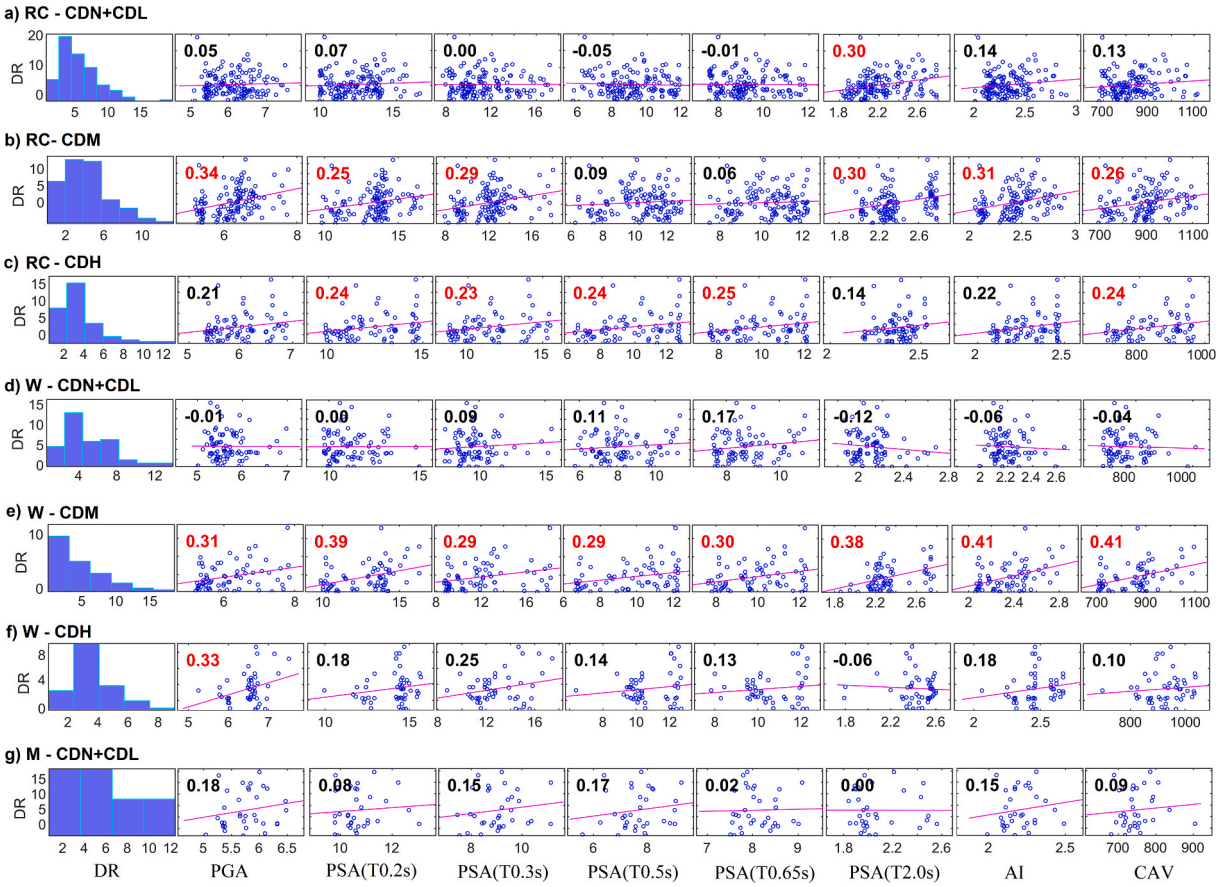

Fig. 6. Correlation between EBK-based IMs (m/s^2) and DRs associated with the 2008 Ölfus earthquake at residential building locations in Hveragerði, corresponding to seven building groups (a–g). Damage ratio histogram for DR $\leq$ 20% is indicated in the leftmost panel. We note that DR $>$ 20% are excluded from the computation as they acted as outlier due to very few numbers.

with the results of a scenario-based risk assessment for Hveragerði, considering the most recent local vs. global fragility functions, and in two levels of municipality vs. building-by-building spatial resolution.

To this end, first, having the complete information about the building portfolio in the detailed exposure database, the key building typologies are identified according to the SERA taxonomy system [61] proposed by the European Seismic Risk Model 2020 (ESRM20). It should be noted that the exposure database provided in the present study is in a high level of detail (level 2). Buildings are classified into eight main typologies (see Table 3) based on the expected level of ductility, construction material, LLRS, number of storey as well as expert judgment. The standard construction materials are reinforced concrete (CR), timber (W), and unreinforced masonry with concrete blocks (MUR + CB). The ductility level reflects different levels of seismic design. Herein, the CR structures are divided into two ductility levels. Namely, low ductility structures were built before 1976 that incorporated minimal seismic provision and medium ductility structures that included some seismic design degree and were made after 1976 when the first seismic code was implemented in Iceland. Although the LLRS for almost all buildings is wall (LWAL), for timber buildings, a moment frame (LFM) is believed to be a

Table 3
Building typologies for residential buildings in Hveragerdi according to the SERA taxonomy system.

Typology[a]	CR_LWAL-DUL_H1	CR_LWAL-DUL_H2	CR_LWAL-DUM_H1	CR_LWAL-DUM_H2	W_LFM-DUM_H1	W_LFM-DUM_H2	MUR-CB99_LWAL-DNO_H1	MUR-CB99_LWAL-DNO_H2
Label	CL1	CL2	CM1	CM2	W1	W2	M1	M2
No. buildings	127	30	240	24	268	20	34	14
Average economic cost[b]	177,2 ± 8,1	154,8 ± 17,3	192,0 ± 15,9	169,5 ± 17,0	174,3 ± 20,3	156,6 ± 18,7	156,1 ± 13,0	152,4 ± 15,7

[a] The building typologies are selected in accordance with building classes for which global fragility functions were available.
[b] The average economic cost values are given in Icelandic Krona (1000 ISK) per m^2 area floor for new construction (1 Euro = 150 ISK).

more appropriate LLRS. The reason is the limited available fragility functions for wood buildings in the global library of fragility models (the fragility models associated with LWAL LLRS were considerably different from the reality). A few numbers of existing 3-storey buildings are classified as 2-storey building class (H2). Based on the local engineering expert opinion in Iceland, structures built before 2008 are designed based on less rigorous regulations than modern seismic codes; thereby, no buildings are classified as high ductility. This is in fact the same conclusion as in a recent article about the building stock in Europe (Crowley et al. [53]). Table 3 presents the identified model building typologies for Hveragerði building stock, their associated short names, and the distribution of the number of buildings within each typology. The most prominent building typologies in Hveragerði are W-LFM-DUM-H1, CR-LWAL-DUM-H1, and then CR-LWAL-DUL-H1 with 35.4%, 31.7%, and 16.77% of the building stock, respectively. Neglecting the ductility level and building height, CR-LWAL class is the prominent class (see also Fig. 5).

The significant spatial variation of the IMs over the small study area illustrates that the assumption of uniform distribution of a single ground motion parameter for a relatively small cell in seismic risk assessment can give deceptive results. Hence, we stress the necessity of conducting a seismic risk assessment for local areas at the highest geographical resolution, i.e., building-by-building, as conducted in the following. The results are compared with the loss estimates performed at a municipality level, i.e., a grid cell area of ~2 km by 2 km, which is smaller than the area commonly used in regional loss modeling.

Furthermore, to have a more reliable and informed view of the seismic risk, we carry out the loss estimation using a logic-tree framework where we introduce the two sources of uncertainties, namely: replacement value (monetary building values) and ground shaking IM. For high-resolution loss estimation (i.e., building-by-building), we employ the statistics of the inferred spectral-based IMs at building coordinates across Hveragerði obtained from their corresponding EBK-based shakemaps associated with PGA and PSAs at short periods. Therefore, ground shaking values are provided in three logic-tree branches: the mean IM, upper bound IM, and lower bound IM, which is calculated by mean ± one standard deviation, with weights of 70%, 15%, and 15%. However, for loss estimation at the municipality level, the statistics of PGA and PSAs at recording stations are employed to determine the same three logic tree branches with the same weights as for the high-resolution loss estimation. Moreover, all buildings' information necessary for risk assessment is aggregated.

To determine the economic cost, first, the replacement value for each building (dwelling) is normalized by the floor area. The mean and standard deviation of the normalized economic values are calculated for the whole Hveragerði, corresponding to each building typology (see Table 3). Having the statistic of the economic values (known as monetary values), three branches are defined considering the mean, mean - standard deviation (lower bound of the economic value), and mean + standard deviation (upper bound of the economic values) and hence incorporated within the logic-tree framework with weights of 60%, 20%, and 20%. Moreover, the mean loss value corresponding to the complete, extensive, moderate, and slight damage states (DS) are determined by 100%, 60%, 20%, and 5% of the total normalized monetary values to be consistent with the damage-to-loss model used to derive global vulnerability functions in terms of direct economic loss by Martins and Silva (see Table 2 of [62]). The mean economic cost per square meter ranges from 154.8 to 192 thousand ISK/m^2 for RC structures, 156 to 174 thousand ISK/m^2 for timber buildings, and 152 to 156 thousand ISK/m^2 for masonry buildings. The replacement cost values are reported by Registers Iceland (2020) (see Table 3).

5.2. Local vs. Global fragility and vulnerability models

Martins and Silva [62], hereafter MS20, developed a large databank of fragility functions covering the most common building typologies throughout the world. The MS20 global fragility functions were generated using nonlinear time history analysis on a single degree of freedom. Four damage states (i.e., slight, moderate, extensive, and complete) dependent on the spectral displacement at the yielding point and the ultimate displacement were used to develop the fragility functions. These damage states are based on Lagomarsino and Giovinazzi's [63] proposal with minor modifications preventing crossing between the damage thresholds. The global fragility models associated with the identified building typologies (Table 3) are employed for the risk assessment. Considering the low-rise buildings in Hveragerði and their respective dynamic properties, the fragility models attributed to either PGA or PSA at 0.3 s are utilized depending on the building's natural period and availability of the fragility model.

Two empirical local vulnerability/fragility models exist, ICE2000 and ICE2008 which are both as a function of PGA and developed based on zero-inflated beta regression [34]. The ICE2000 model is calibrated from the observed losses in the South Iceland June 2000 earthquakes while the ICE2008 model is calibrated using loss data from the May 2008 earthquake. Both models give parameter sets for five building typologies, namely, CR + CIP[1] – CDN + CDL, CR + CIP – CDM + CDH, W + WLI[2] – CDN + CDL, W + WLI – CDM + CDH, and MR + CBH[3]+MOC[4] – CDN + CDL (see Ref. [64]). All typologies are restricted to LWAL LLRS and low-rise buildings with one or two stories (HBET:2,1). Bessason et al. [34] recommended using the ICE2000 model to predict losses for earthquakes in the M_w range 6.4–6.6 and the ICE2008 model for events in the M_w range 6.2–6.4. In this study, both models are used for the scenario earthquake for Hveragerði. Fig. 7 presents a visual comparison of global fragility function with the local ones for the low-code RC building typology used for risk analysis in this study. Fig. 7a corresponds to CL1 and CL2 (see Table 3) for one and two-storey low-code RC buildings with LWAL LLRS. Fig. 7b presents both existing local models of ICE2000 and ICE2008 for "CR + CIP – CDN + CDL" no-code and low-code RC building class. The fragility functions are provided for four damage states distinguished by different colors in legend. The significant difference amongst global and local models is apparent at all damage states. Furthermore, ICE2000 and ICE2008 models depicted by

[1] CIP: Cast-in-place.
[2] WLI: Light-wood-members.
[3] CBH: Concrete-blocks-hollow.
[4] MOC: Cement mortar.

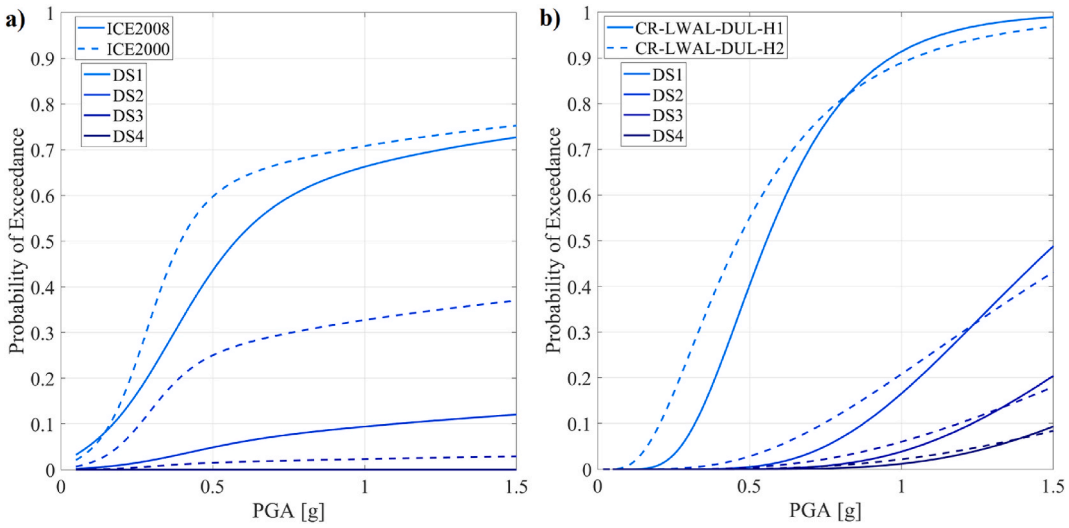

Fig. 7. Example of fragility functions in PGA (g) for a low-rise RC building typology used in this study, a) local fragility curves of ICE2000 and ICE2008, and b) MS20 global fragility functions of CL1 and CL2.

solid and dashed lines, respectively (Fig. 7a) indicate remarkable discrepancy, especially for DS2.

It should be noted that the fragility and vulnerability models adopted in this study do not account for the pulse-like effect. According to recent studies ([65,66]), the effects of pulse-like ground motions on seismic demands and resulting fragility of short-period structures, which is the key characteristic of the building assets in this study, are not particularly significant since directivity-induced pulses are generally long-period phenomena. Additionally, pulse-like ground motions are practically not affecting the slight and moderate damage fragility relationships, for which an essentially-elastic behavior is expected. Instead, for the damage states involving non-linear behavior (extensive and complete damage), such effect is somehow proportional to the ductility capacity of the case study; in other words, the reduction in median fragility caused by pulse-like ground motions is higher for structures with larger ductility capacity. Thus, this study does not investigate the impact of the directivity-induced pulse-like ground motions on building loss assessment.

To predict possible losses, the open-source earthquake risk and loss assessment tool, SEismic Loss EstimatioN using a logic tree Approach (SELENA) [33] is employed. Eventually, we calculate a number of relevant risk metrics, namely, the total economic loss value MDR for each building typology expressed as the ratio of damage cost to the cost of new construction, and finally, damage probabilities at five damage states and for each building typology.

5.3. Loss estimation results

The mean total economic losses caused by Ölfus earthquake scenario on residential buildings in Hveragerði is estimated at 1459 million Icelandic Krona (ISK) with 16^{th} and 84^{th} percentile of 1330 and 1588 million ISK based on risk calculation at the building-by-building level. Also, regarding municipality level risk calculation, the mean economic loss value of 1478.5 million ISK is estimated from the aggregation of economic losses corresponding to each building with 16^{th} and 84^{th} percentile of 1350 and 1608 million ISK. The actual repair cost paid by the insurance company to building owners was about 750 million ISK, which is significantly lower than the MS20 predicted values. The local ICE2008 model estimated 934 million ISK loss value which is close to the real repair cost. Whilst the ICE2000 model predicts 1905.4 million ISK. The discrepancy between the risk assessment results of the two local models can stem from different reasons. Bessason et al. [34] concluded that the energy content and duration of the ground motion, reflected by magnitude size, are of importance, and these factors are not mirrored by the PGA parameter alone.

Looking in more detail at the predicted and observed losses, Fig. 8a presents the repair-to-replacement cost ratio (MDR) for eight building typologies predicted using MS20 fragility models in two resolution levels, namely, the classical municipality level (classical resolution prediction, orange bars) and high-resolution of building-by-building (high-resolution prediction, blue bars). For the MS20 model, a dispersion/variability in damage ratios must be considered by the logic tree branch when loss results are used to develop risk management strategies. Therefore, herein, the 84^{th} and 16^{th} percentiles of the estimated MDRs are indicated by error bars. To compare the loss estimates with ones calculated from the observed repair costs after the May 2008 earthquake, the observed MDRs corresponding to each typology is shown by yellow bars.

In accordance with our expectation, building typologies associated with low ductility (e.g., CL1, CL2) results in higher loss than buildings with higher ductility (e.g., CM1, CM2) (see Fig. 8a), although the differences are not large for observed data. Moreover, for CL1 and CM1 which includes 48% of residential buildings in Hveragerði, the MDR predictions are slightly lower than the observed MDRs. While for the remaining typologies, the predicted MDRs are generally (much) larger than the observed ones. Note that by multiplying the MDR estimates illustrated in Fig. 8a by the replacement costs reported in Table 3, and floor area, the repair cost associated with each building typology can be obtained.

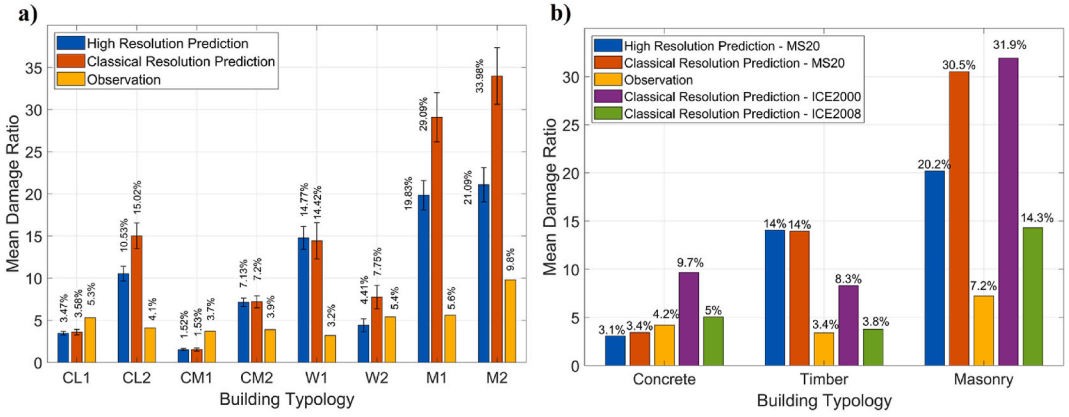

Fig. 8. a) Mean damage ratio (MDR) for eight building typologies predicted using MS20 fragility models, in classical municipality level (orange bars) and high-resolution of building-by-building (blue bars), along with its 84th and 16th percentiles (error bars), as well as the MDR from observed loss values (yellow bars). b) MDR for three building classes, predicted by MS20 fragility models, ICE2000 and ICE2008 local models, and their comparison with corresponding observed losses.

Additionally, in Fig. 8b, we evaluate the performance of ICE2000 and ICE2008 local models and their comparison with MS20 and observed MDRs for three building classes of concrete, timber, and masonry. To have an acceptable comparison, the MDR predictions relative to eight and five building typologies associated with MS20 and local models, respectively, are weighted based on the number of buildings in each class.

If the observed MDRs are pooled for three main groups of concrete, timber, and masonry buildings, then the observed MDRs for each group are 4.2%, 3.4% and 7.2%, respectively (See Fig. 8b). Therefore, the observed data indicates that masonry buildings are the most vulnerable building class with the highest observed MDR. Moreover, the timber and concrete buildings displayed the best performance during the earthquake. When Ölfus earthquakes struck in May 2008, less than 7% of the residential buildings were

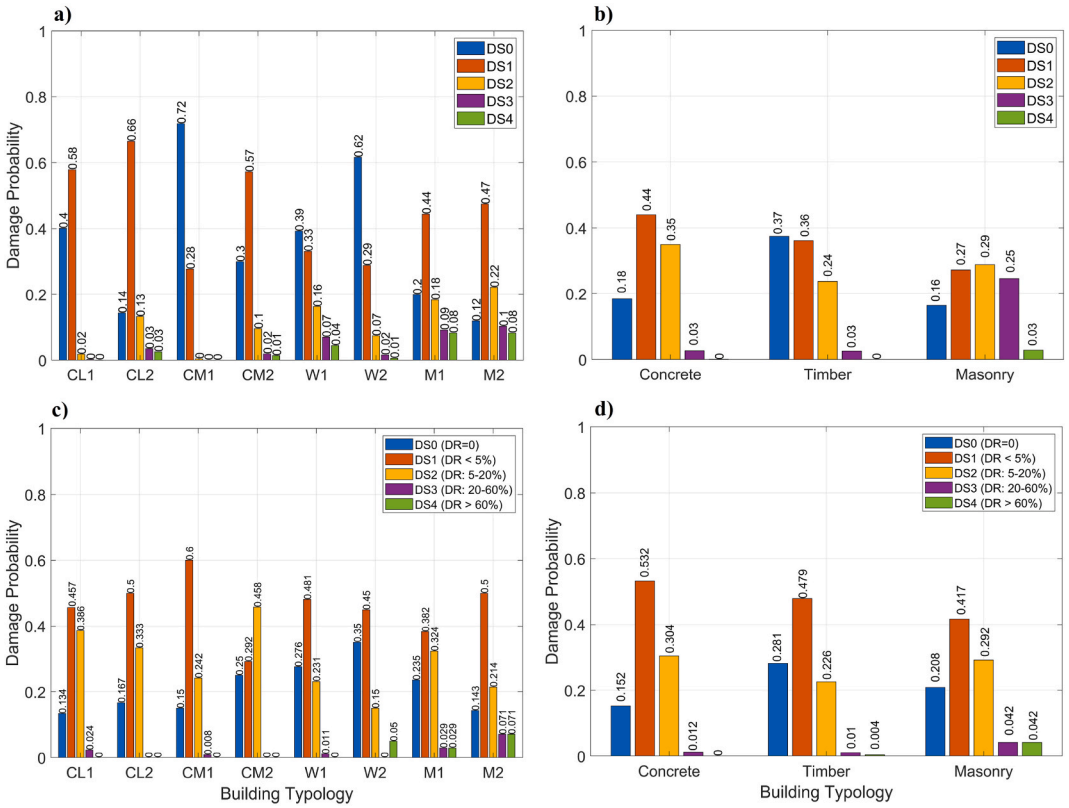

Fig. 9. Damage probability for Hveragerði based on (a) high-resolution risk assessment using eight global fragility models proposed by MS20, (b) classical spatial-resolution risk assessment using local fragility model of ICE2008 for three material categories of buildings, and (c) observed losses classified using the SERA taxonomy system, vs. (d) observed losses based on the three material categories of buildings.

masonry buildings, and they are no longer constructed in Iceland, which will help to reduce the risk in future earthquakes.

For timber building class, the Icelandic vulnerability models, especially ICE2008, predict well the observed damage in Hveragerði. While global fragility functions tend to greatly overestimate the losses of timber buildings. For concrete buildings, the MS20 and ICE2008 models predict the observed MDR with slight discrepancy. For masonry buildings, the global and both local models significantly overpredict the observation, although the similarity of results between the classical MS20 and ICE2000 predictions is noteworthy.

Based on MS20 predictions, the least vulnerable buildings are those made of reinforced concrete with wall LLRS, in particular with medium ductility as illustrated by the small loss predictions associated with CM1 and CM2 in Fig. 8a. Whereas, based on ICE2000 and ICE2008 models, the timber building class with the smallest MDR is the least vulnerable one.

The total weighted MDR for the whole Hveragerði is estimated at 8.33% and 5.11% using the building-by-building resolution MS20 and ICE2008 models, respectively. Considering the total observed MDRs of 4.1%, the local ICE2008 model acts superior in predicting the total MDR for all buildings in Hveragerði. Overall, the ICE2008 model performs superior in estimating damages to timber and concrete buildings across Hveragerði.

According to Fig. 8, the MDR estimates associated with municipality resolution level in the loss estimation overestimate the ones from building-by-building resolution for about half of the typologies. For one-storey typologies comprising large number of buildings such as CL1, CM1, and W1, the estimates are quite similar. For masonry building classes (M1 and M2), high-resolution MDR estimates are significantly lower, and thus, with less discrepancy with observed MDR. However, we emphasize that in high- and low-resolution risk assessment conducted in this study, the spatial variability of IMs in the study area was captured through adopting specific logic tree branches for their corresponding median, lower and upper bound values.

Fig. 9 presents the damage probability for five damage states determined by independent MS20 fragility functions (Fig. 9a) as well as ICE2008 fragility models (Fig. 9b). According to Fig. 9a, the probability of extensive damage (DS3, purple bars) or collapse (DS4, green bars) in reinforced concrete buildings is almost zero; 7% and 4% in W1; and 9% and 8% in M1, respectively. Note that the MS20 predictions (Fig. 9a) are from high-resolution risk assessment, which differs slightly from the classical-resolution risk calculation. To scrutinize, there is a negligible difference for CL1, CL2, CM1, and CM2 typologies, whereas the discrepancy is more apparent for M1 and M2 with larger moderate to complete damage estimates in classical risk assessment (lower resolution).

The ICE2008 vulnerability model can be used to create fragility curves for any damage state as long they are defined for specific loss bins [34]. Therefore, to have a fair comparison, ICE2008 fragility curves are reconstructed in this study for loss bins which are considered to be consistent with the damage states utilized by MS20: DS0 - No damage, DR $= 0$; DS1 - Slight damage, $0 < \mathrm{DR} \leq 5\%$; DS2 - Moderate damage, $5\% < \mathrm{DR} \leq 20\%$; DS3 - Extensive damage $20\% < \mathrm{DR} \leq 60\%$, and DS4 - Collapse, $60\% < \mathrm{DR} \leq 100\%$. On this basis, the ICE2008 model predicts a 3% probability of extensive damages for concrete and timber and 25% for masonry which is larger than MS20 predictions (~10%). It is of interest that MS20 estimates 7% and 4% probability of extensive damage and collapse in the W1 class which includes 93% of timber buildings.

Fig. 9c and d show observed damage states in different building classes after the Ölfus earthquake which are comparable to the predicted damage states in the upper panels. Fig. 8d depicts that about 68.4% of RC buildings, 76% of timber, and 62.5% of masonry buildings experienced no or slight damages ($\mathrm{DR} < 5\%$) (DS0 and DS1). Furthermore, 1.2%, 1.4%, and 8.4% of RC, timber and masonry buildings suffered extensive ($20\% < \mathrm{DR} < 60\%$) or complete damages ($\mathrm{DR} > 60\%$) after Ölfus earthquake, respectively. The highest damage probability was observed mostly in old residential areas of Hveragerði as per our expectation. To be more specific, out of seven highly damaged buildings with $\mathrm{DR} > 20\%$, one was two-storey timber with 100% DR built in 1950 (see W2-DS4 in Fig. 9c), three of them were masonry built in 1940–1950, and the remaining three were one-storey concrete buildings (two constructed in 1974 in CL1 and one in 1977 in CM1, see DS3 in Fig. 8c). These can also be validated by detailed classified damage probability illustrated in Fig. 9c.

Moderate damage predictions (DS2) obtained from global fragility functions (Fig. 9a) are smaller than their corresponding observations (Fig. 9c) with the prediction-to-observation ratio ranging from zero and 1/10th from CM1 and CL1 toward less discrepancy of ~50% seen in W2 and M1 and finally 70% in W1. This is contrary to the performance of local model predictions in DS2 where there is a great agreement between predicted (Fig. 9b) and observed damage probabilities (Fig. 9d). Moreover, for no damage and slight damage state groups, the discrepancy between observed damages and the predictions determined from local fragility models are smaller than those obtained from MS20 global fragility models.

Finally, comparing MS20 predictions in extensive to collapse damage states with their corresponding observations indicate the excellent seismic resistance of buildings in Hveragerði which can be due to the fact that the Icelandic buildings are constructed to withstand substantial lateral loads imposed by winds because the prescribed wind force loads in Iceland are among the highest in Europe. The fundamental base value of wind velocity is $v_{b,0} = 36$ m/s (CEN, 2005; Icelandic standards, 2010). Additionally, for all building typologies, the floor slabs and the building foundations are built using reinforced concrete that ties the foundations together and makes them more earthquake resistant. It is worth emphasizing that as explained above the consequences of a specific earthquake scenario can change remarkably depending on the earthquake characteristics such as magnitude, ground motion intensity, the distance between the earthquake source and the assets at risk, site condition of exposed assets and so forth.

6. Summary and conclusions

In this study, we take advantage of the intense high-frequency ground accelerations and large amplitude and long-period near-fault pulses during the M_w6.3, May 29, 2008 Ölfus earthquake in Southwest Iceland that were recorded on the dense strong-motion array (ICEARRAY I) in the small urban area of Hveragerði that was in the extreme near-fault region of the earthquake. The observed horizontal PGA of approximately 40%–90% g was ~ 2–4.5 times higher than the design requirements of the vast majority of the buildings

in Hveragerði. Fortunately, however, there were no building collapses and no loss of life. Nevertheless, the town suffered significant damage and therefore a comprehensive GIS-based building exposure database for the town was collated and linked to the loss database (i.e., repair cost) provided by the Natural Catastrophe Insurance of Iceland on a dwelling-by-dwelling level.

In order to assign each building in Hveragerði an IM value and inspect the spatial variations of the IMs across the town, we generate high-resolution shakemaps for a set of well-known seismic ground motion intensity measures including PGA, PSAs at short-to-long periods and two energy-based IMs, i.e., AI and CAV from the ICEARRAY I acceleration time histories, applying empirical Bayesian kriging geostatistical analysis. The EBK-based shakemaps showed significant and systematic variation of the IMs across the small study area. In general, for IMs at short and intermediate periods, the lowest amplitudes were observed in the center of town with the highest in the outskirts, which can in part be explained by local geological features. Moreover, considerable IM variability was observed at higher frequency ground motions, while long-period motions showed near none, with the exception of the different spatial patterns of fault-parallel and fault-normal velocity pulses at intermediate periods. The long-period PSA shakemap showed small amplitude level, with the E-W component having much higher ones due to the broad-band nature of the forward directivity pulse. The AI and CAV shakemaps appear to capture the salient features of all PGA and low-period PSAs.

Correlation analysis was carried out for the building data in various groups classified by the status of the active seismic code upon their construction and damage ratios calculated from the loss data for each building. Overall, it's been demonstrated that PGA is not the best overall IM that correlated with damage ratio. The systematic pattern of IM amplitudes did not however appear to be manifested in the high-spatial resolution building-specific damage ratios. In general, low correlations were observed except for a few groups showing moderate correlations (e.g., RC-CDM and W-CDM). This can partially be explained by the fact that the observations of the in-situ survey of the damaged buildings conducted after the Ölfus earthquake showed that the non-structural components were the primary elements that were damaged and not the structural elements, for which the code design requirements specifically apply. Furthermore, the seismic performance of the structural elements of the primarily residential buildings in Hveragerði can be attributed to the abundance of low-rise one-storey single buildings with light roofs, symmetric and regular design in plan and height, as well as well-designed structural walls LLRS. Moreover, the buildings appear to have residual strength not associated with advanced seismic design but other factors (e.g., cold climate and strong wind loads) that resist the earthquake action and thus mitigate potential seismic damage to the structural systems.

As one of the main objectives of this study, we carried out seismic loss assessment in Hveragerði for the Ölfus earthquake scenario. To this end, residential buildings were classified into eight building typologies as per the SERA taxonomy scheme. The global fragility functions proposed by Martins and Silva [62] as part of global risk modellng ([67]) along with the most recent empirical local models [34] were employed corresponding to each building typology in a logic-tree framework for handling the uncertainty. The predicted risk metrics were compared with the observed loss data recorded following the Ölfus earthquake.

Overall, masonry buildings are the most vulnerable building typology with the most considerable expected losses. The global fragility functions significantly overestimate the observed losses for all building typologies, except for one-story reinforced concrete buildings. On the other hand, the local empirical model of ICE2008 performed well in predicting the seismic performance of the timber and concrete building stocks during the Ölfus earthquake. Finally, we evaluated the seismic losses for a high-spatial resolution (building-by-building level) exposure dataset and compared them with those obtained from a classical municipality level resolution, defined by a small grid cell. In half of the cases, the high-resolution predictions gave results that better correlated with the observed losses. In the other cases, both levels gave similar results.

Our comparison between local and global models indicates that when a large-scale vulnerability estimation is carried out the use of global fragility functions tend to overestimate the losses of region-specific building typologies (e.g., timber structures for Iceland) but it provides good results for typical structures (e.g., low-rise RC buildings). In terms of total economic losses caused by Ölfus earthquake scenario on residential buildings in Hveragerði, both global and local ICE2000 models overestimate the actual repair cost paid by the insurance company by about twofold. Whilst the ICE2008 model predicted economic losses close to the actual repair cost. The discrepancy between the risk assessment results of the two local models can stem from the differences in energy content and duration of the ground motion, reflected by magnitude size which are not reflected by the PGA parameter alone. Caution is needed when using an empirical vulnerability model to predict losses for magnitudes different from the size of the destructive earthquake that was used to calibrate the model.

This study has pushed the limits of a data-driven high-spatial-resolution loss estimation. Namely, it is enabled by the high-resolution database of not only exposure data, but also intensity measures from a dense urban array of strong-motion stations that recorded significant and damaging seismic ground motions, along with a building-by-building loss data for the earthquake scenario used. It has showcased the physics-guided analysis of the intense near-fault ground motions and the corresponding calculations of multiple IMs and their interpretation. Finally, the loss estimation has shown the futility of using only global vulnerability or fragility models for the Icelandic building stock which has repeatedly shown very low vulnerability to even strong seismic motions.

Declaration of competing interest

The authors declare that they have no known competing financial interests or personal relationships that could have appeared to influence the work reported in this paper.

Acknowledgements

This study was funded by the TURNkey H2020 European project (Towards more Earthquake-Resilient Urban Societies through a Multi-Sensor-Based Information System enabling Earthquake Forecasting, Early Warning and Rapid Response Actions) [www.

earthquake-turnkey.eu] under grant agreement No 821046. This work was facilitated by an Erasmus+ staff mobility grant No. IS-TS2020-87850 for the lead author to the University of Alicante, Spain. This work was also partly supported by a Postdoctoral fellowship (No. 218255-051) and grant of excellence (No. 218149-051) from the Icelandic Research Fund of the Icelandic Centre for Research, and the University of Iceland Research Fund. The authors thank the Natural Catastrophe Insurance of Iceland (http://www.nti.is/en/) for providing the building damage database for the 2008 earthquake. Furthermore, we are grateful to the Registers Iceland (https://www.skra.is/english/) for making the building properties database of Hveragerði available to the University of Iceland for the purposes of this research. The authors would like to acknowledge the anonymous reviewers who have contributed significantly to improving and enriching the paper.

References

[1] P. Einarsson, Earthquakes and present-day tectonism in Iceland, Tectonophysics 189 (1991) 261–279.
[2] P. Einarsson, Mechanisms of earthquakes in Iceland, in: M. Beer, I.A. Kougioumtzoglou, E. Patelli, I.S.-K. Au (Eds.), Encyclopedia of Earthquake Engineering, Springer Berlin Heidelberg, Berlin, Heidelberg, 2014, pp. 1–15, https://doi.org/10.1007/978-3-642-36197-5_298-1.
[3] R. Stefánsson, R. Böðvarsson, R. Slunga, P. Einarsson, S. Jakobsdóttir, H. Bungum, S. Gregersen, J. Havskov, J. Hjelme, H. Korhonen, Earthquake prediction research in the South Iceland seismic zone and the SIL project, Bull. Seismol. Soc. Am. 83 (1993) 696–716.
[4] R. Stefánsson, G.B. Guðmundsson, P. Halldórsson, Tjörnes fracture zone. New and old seismic evidences for the link between the North Iceland rift zone and the Mid-Atlantic ridge, Tectonophysics 447 (2008) 117–126.
[5] P. Einarsson, Á.R. Hjartardóttir, S. Hreinsdóttir, P. Imsland, The structure of seismogenic strike-slip faults in the eastern part of the Reykjanes Peninsula Oblique Rift, SW Iceland, J. Volcanol. Geoth. Res. 391 (2020) 106372.
[6] L. Steigerwald, P. Einarsson, Á.R. Hjartardóttir, Fault kinematics at the Hengill Triple Junction, SW-Iceland, derived from surface fracture pattern, J. Volcanol. Geoth. Res. 391 (2020) 106439, https://doi.org/10.1016/j.jvolgeores.2018.08.017.
[7] Standards Council of Iceland/Staðlaráð Íslands (SI), Icelandic National Annexes to EUROCODES, Staðlaráð Íslands, Reykjavík, Iceland, 2010.
[8] J. Decriem, T. Arnadottir, A. Hooper, H. Geirsson, F. Sigmundsson, M. Keiding, B.G. Ofeigsson, S. Hreinsdottir, P. Einarsson, P. LaFemina, R.A. Bennett, The 2008 May 29 earthquake doublet in SWIceland, Geophys. J. Int. 181 (2010) 1128–1146.
[9] B. Halldorsson, R. Sigbjörnsson, R. Rupakhety, A.A. Chanerley, Extreme near-fault strong-motion of the M6.3 Ölfus earthquake of 29 May 2008 in South Iceland, in: 14th European Conference on Earthquake Engineering (14ECEE), Ohrid, Macedonia, 2010, p. 1640. Paper no.
[10] B. Halldorsson, R. Sigbjörnsson, The Mw6.3 Ölfus earthquake at 15:45 UTC on 29 May 2008 in South Iceland: ICEARRAY strong-motion recordings, Soil Dynam. Earthq. Eng. 29 (2009) 1073–1083.
[11] B. Halldorsson, R. Sigbjörnsson, A.A. Chanerley, N.A. Alexander, Near-fault strong-motion array recordings of the Mw6.3 Ölfus earthquake on 29 May 2008 in Iceland, in: 9th US National and 10th Canadian Conference on Earthquake Engineering (9USN/10CCEE), Canada, Toronto, 2010. Paper no. 1157.
[12] R. Sigbjörnsson, R. Rupakhety, B. Halldorsson, J.Th Snæbjörnsson, On the modelling of incoherence of strong-motion: a study of the May 2008 Ölfus earthquake, in: Proceedings of the 2nd European Conference on Earthquake and Engineering Seismology (2ECEES), Istanbul, Turkey, 2014.
[13] S. Rahpeyma, B. Halldorsson, B. Hrafnkelsson, S. Jónsson, Bayesian hierarchical model for variations in earthquake peak ground acceleration within small-aperture arrays, Environmetrics 29 (2018) e2497, https://doi.org/10.1002/env.2497.
[14] S. Rahpeyma, B. Halldorsson, B. Hrafnkelsson, S. Jónsson, S. Jonsson, Frequency Dependent Site Factors for the Icelandic Strong-Motion Array from a Bayesian Hierarchical Model of the Spatial Distribution of Spectral Accelerations, Earthquake Spectra, 2021, https://doi.org/10.1177/87552930211036921.
[15] G.A. Weatherill, V. Silva, H. Crowley, P. Bazzurro, Exploring the impact of spatial correlations and uncertainties for portfolio analysis in probabilistic seismic loss estimation, Bull. Earthq. Eng. 13 (2015) 957–981.
[16] J. Park, P. Bazzurro, J.W. Baker, Modeling Spatial Correlation of Ground Motion Intensity Measures for Regional Seismic Hazard and Portfolio Loss Estimation, Applications of Statistics and Probability in Civil Engineering, 2007, pp. 1–8.
[17] N. Jayaram, J.W. Baker, Correlation model for spatially distributed ground-motion intensities, Earthq. Eng. Struct. Dynam. 38 (2009) 1687–1708, https://doi.org/10.1002/eqe.922.
[18] K. Goda, Interevent variability of spatial correlation of peak ground motions and response Spectra Short note, Bull. Seismol. Soc. Am. 101 (2011) 2522–2531, https://doi.org/10.1785/0120110092.
[19] V. Sokolov, F. Wenzel, Influence of spatial correlation of strong ground motion on uncertainty in earthquake loss estimation, Earthq. Eng. Struct. Dynam. 40 (2011) 993–1009, https://doi.org/10.1002/eqe.1074.
[20] A. Miano, F. Jalayer, G. Forte, A. Santo, Empirical fragility assessment using conditional GMPE-based ground shaking fields: application to damage data for 2016 Amatrice Earthquake, Bull. Earthq. Eng. 18 (2020) 6629–6659, https://doi.org/10.1007/s10518-020-00945-6.
[21] A. Miano, F. Jalayer, R. De Risi, A. Prota, G. Manfredi, Model updating and seismic loss assessment for a portfolio of bridges, Bull. Earthq. Eng. 14 (2016) 699–719, https://doi.org/10.1007/s10518-015-9850-y.
[22] J.R. Carr, E.D. Deng, C.E. Glass, An application of disjunctive kriging for earthquake ground motion estimation, Math. Geol. 18 (1986) 197–213, https://doi.org/10.1007/BF00898283.
[23] S.-S. Jeon, T.D. O'Rourke, Northridge earthquake effects on pipelines and residential buildings, Bull. Seismol. Soc. Am. 95 (2005) 294–318, https://doi.org/10.1785/0120040020.
[24] C.B. Worden, E.M. Thompson, J.W. Baker, B.A. Bradley, N. Luco, D.J. Wald, Spatial and spectral interpolation of ground-motion intensity measure observations, Bull. Seismol. Soc. Am. 108 (2018) 866–875, https://doi.org/10.1785/0120170201.
[25] A. Costanzo, Shaking maps based on cumulative absolute velocity and Arias intensity: the cases of the two strongest earthquakes of the 2016–2017 Central Italy seismic sequence, IJGI 7 (2018) 244, https://doi.org/10.3390/ijgi7070244.
[26] J.W. Baker, Y. Chen, Ground motion spatial correlation fitting methods and estimation uncertainty, Earthq. Eng. Struct. Dynam. 49 (2020) 1662–1681, https://doi.org/10.1002/eqe.3322.
[27] R. Gentile, C. Galasso, Gaussian process regression for seismic fragility assessment of building portfolios, Struct. Saf. 87 (2020) 101980, https://doi.org/10.1016/j.strusafe.2020.101980.
[28] Y.-M. Wu, D.-Y. Chen, T.-L. Lin, C.-Y. Hsieh, T.-L. Chin, W.-Y. Chang, W.-S. Li, S.-H. Ker, A high-density seismic network for earthquake early warning in Taiwan based on low cost sensors, Seismol Res. Lett. 84 (2013) 1048–1054, https://doi.org/10.1785/0220130085.
[29] R. Rupakhety, R. Sigbjörnsson, S. Ólafsson, Damage to residential buildings in Hveragerði during the 2008 Ölfus Earthquake: simulated and surveyed results, Bull. Earthq. Eng. 14 (2016) 1945–1955, https://doi.org/10.1007/s10518-015-9783-5.
[30] R. Sigbjörnsson, S. Ólafsson, J.Th Snæbjörnsson, Macroseismic effects related to strong ground motion: a study of the South Iceland earthquakes in June 2000, Bull. Earthq. Eng. 5 (2007) 591–608, https://doi.org/10.1007/s10518-007-9045-2.
[31] K. Jónasson, B. Bessason, Á. Helgadóttir, P. Einarsson, G.B. Gudmundsson, B. Brandsdóttir, K.S. Vogfjörd, K. Jónsdóttir, A harmonised instrumental earthquake catalogue for Iceland and the northern Mid-Atlantic Ridge, Nat. Hazards Earth Syst. Sci. Discuss. (2021) 1–26.
[32] J.Ö. Bjarnason, P. Einarsson, B. Bessason, Iceland catastrophe insurance and earthquake risk assessment, in: International Workshop on Earthquakes in North Iceland. Húsavík, North Iceland, 2016.
[33] S. Molina, D.H. Lang, C.D. Lindholm, Selena - an open-source tool for seismic risk and loss assessment using a logic tree computation procedure, Comput. Geosci. 36 (2010) 257–269, https://doi.org/10.1016/j.cageo.2009.07.006.
[34] B. Bessason, R. Rupakhety, J.Ö. Bjarnason, Comparison and modelling of building losses in South Iceland caused by different size earthquakes, J. Build. Eng. 46 (2022) 103806, https://doi.org/10.1016/j.jobe.2021.103806.

[35] R. Sigbjörnsson, J.T. Snæbjörnsson, S.M. Higgins, B. Halldórsson, S. Ólafsson, A Note on the M W 6.3 Earthquake in Iceland on 29 May 2008 at 15:45 UTC, Bulletin of Earthquake Engineering, 2009, https://doi.org/10.1007/s10518-008-9087-0.
[36] B. Halldorsson, R. Sigbjornsson, J. Schweitzer, ICEARRAY: the first small-aperture, strong-motion array in Iceland, J. Seismol. 13 (2009) 173–178.
[37] S. Hreinsdóttir, T. Árnadóttir, J. Decriem, H. Geirsson, A. Tryggvason, R.A. Bennett, P. LaFemina, A complex earthquake sequence captured by the continuous GPS network in SW Iceland, Geophys. Res. Lett. 36 (2009) L12309.
[38] R. Rupakhety, B. Halldorsson, R. Sigbjörnsson, Estimating coseismic deformations from near source strong motion records: methods and case studies, Bull. Earthq. Eng. 8 (2010) 787–811, https://doi.org/10.1007/s10518-009-9167-9.
[39] G.P. Mavroeidis, A.S. Papageorgiou, Near-source strong ground motion: characteristics and design issues, in: Proc. Of the Seventh US National Conf. on Earthquake Engineering (7NCEE), Boston, MA, USA, 2002, p. 25.
[40] G. Mandl, Tectonic deformation by rotating parallel faults: the "bookshelf" mechanism, Tectonophysics 141 (1987) 277–316, https://doi.org/10.1016/0040-1951(87)90205-8.
[41] F. Sigmundsson, P. Einarsson, R. Bilham, E. Sturkell, Rift-transform kinematics in South Iceland: deformation from global positioning system measurements, 1986 to 1992, J. Geophys. Res. Solid Earth 100 (1995) 6235–6248, https://doi.org/10.1029/95JB00155.
[42] S. Jónsson, Importance of post-seismic viscous relaxation in southern Iceland, Nat. Geosci. 1 (2008) 136–139.
[43] W.H.K. Lee, H. Kanamori, P. Jennings, C. Kisslinger, International Handbook of Earthquake & Engineering Seismology, Academic Press, 2003.
[44] N.A. Abrahamson, K.M. Shedlock, Overview, Seismol Res. Lett. 68 (1997) 9–23, https://doi.org/10.1785/gssrl.68.1.9.
[45] J. Douglas, Earthquake ground motion estimation using strong-motion records: a review of equations for the estimation of peak ground acceleration and response spectral ordinates, Earth Sci. Rev. 61 (2003) 43–104.
[46] D.M. Boore, J. Watson-Lamprey, N.A. Abrahamson, Orientation-independent measures of ground motion, Bull. Seismol. Soc. Am. 96 (2006) 1502–1511.
[47] D.M. Boore, Orientation-independent, non geometric-mean measures of seismic intensity from two horizontal components of motion, Bull. Seismol. Soc. Am. 100 (2010) 1830–1835.
[48] R. Rupakhety, R. Sigbjörnsson, Rotation-invariant measures of earthquake response spectra, Bull. Earthq. Eng. 11 (2013) 1885–1893.
[49] M. Kowsari, T. Sonnemann, B. Halldorsson, B. Hrafnkelsson, J.þ. Snæbjörnsson, S. Jónsson, Bayesian inference of empirical ground motion models to pseudo-spectral accelerations of South Iceland seismic zone earthquakes based on informative priors, Soil Dynam. Earthq. Eng. 132 (2020) 106075, https://doi.org/10.1016/j.soildyn.2020.106075.
[50] K. Krivoruchko, A. Gribov, Evaluation of empirical Bayesian kriging, Spatial Stat. 32 (2019) 100368, https://doi.org/10.1016/j.spasta.2019.100368.
[51] K. Sæmundsson, S. Kristinsson, Hveragerði. Hitamælingar Í Jarðvegi Og Sprungur (Hveragerði: Soil Temperature Measurements and Faults), Iceland GeoSurvey (ÍSOR), Reykjavík, Iceland, 2005.
[52] S. Rahpeyma, B. Halldorsson, C. Olivera, R.A. Green, S. Jónsson, Detailed site effect estimation in the presence of strong velocity reversals within a small-aperture strong-motion array in Iceland, Soil Dynam. Earthq. Eng. 89 (2016) 136–151, https://doi.org/10.1016/j.soildyn.2016.07.001.
[53] H. Crowley, V. Despotaki, V. Silva, J. Dabbeek, X. Romão, N. Pereira, J.M. Castro, J. Daniell, E. Veliu, H. Bilgin, C. Adam, M. Deyanova, N. Ademović, J. Atalic, E. Riga, A. Karatzetzou, B. Bessason, V. Shendova, A. Tiganescu, D. Toma-Danila, Z. Zugic, S. Akkar, U. Hancilar, Model of seismic design lateral force levels for the existing reinforced concrete European building stock, Bull. Earthq. Eng. 19 (2021) 2839–2865, https://doi.org/10.1007/s10518-021-01083-3.
[54] E. Tryggvason, S. Thoroddsen, S. Thorarinsson, Report on earthquake risk in Iceland, Timarit Verkfraedingafelags Isl. 43 (1958) 81–97.
[55] ÍST 13, Earthquakes, Loads and Design Rules, Icelandic Industrial Development Agency/Idnthróunarstofun Íslands, Reykjavík, Iceland, 1976.
[56] ÍST 13, Earthquakes, Loads and Design Rules, Icelandic Industrial Development Agency/Idnthróunarstofun Íslands, Reykjavík, Iceland, 1989.
[57] Standards Council of Iceland/Staðlaráð Íslands (SI), National Application Documents (NAD) for Iceland, 2002.
[58] B. Bessason, J.Ö. Bjarnason, R. Rupakhety, Statistical modelling of seismic vulnerability of RC, timber and masonry buildings from complete empirical loss data, Eng. Struct. 209 (2020) 109969, https://doi.org/10.1016/j.engstruct.2019.109969.
[59] B. Bessason, J.Ö. Bjarnason, A. Guðmundsson, J. Sólnes, S. Steedman, Analysis of damage data of low-rise buildings subjected to a shallow Mw6.3 earthquake, Soil Dynam. Earthq. Eng. 66 (2014) 89–101, https://doi.org/10.1016/j.soildyn.2014.06.025.
[60] T.J. Kennedy, B. Halldorsson, J.þ. Snaebjörnsson, R.A. Green, Influence of gravel fill on the seismic response characteristics of sites in Iceland, in: Proceedings of the XVII ECSMGE-2019 Geotechnical Engineering Foundation of the Future, Iceland, Reykjavik, 2019, p. 7, https://doi.org/10.32075/17ECSMGE-2019-0471.
[61] H. Crowley, V. Despotaki, D. Rodrigues, V. Silva, D. Toma-Danila, E. Riga, A. Karatzetzou, S. Fotopoulou, Z. Zugic, L. Sousa, S. Ozcebe, P. Gamba, Exposure model for European seismic risk assessment, Earthq. Spectra 36 (2020) 252–273, https://doi.org/10.1177/8755293020919429.
[62] L. Martins, V. Silva, Development of a fragility and vulnerability model for global seismic risk analyses, Bull. Earthq. Eng. (2020), https://doi.org/10.1007/s10518-020-00885-1.
[63] S. Lagomarsino, S. Giovinazzi, Macroseismic and mechanical models for the vulnerability and damage assessment of current buildings, Bull. Earthq. Eng. 4 (2006) 415–443, https://doi.org/10.1007/s10518-006-9024-z.
[64] S. Brzev, C. Scawthorn, A.W. Charleson, L. Allen, M. Greene, K. Jaiswal, V. Silva, GEM Building Taxonomy Version 2.0, GEM Technical Report 2013-02, 2013, p. 188, https://doi.org/10.13117/GEM.EXP-MOD.TR2013.02.
[65] R. Gentile, C. Galasso, Accounting for directivity-induced pulse-like ground motions in building portfolio loss assessment, Bull. Earthq. Eng. 19 (2021) 6303–6328, https://doi.org/10.1007/s10518-020-00950-9.
[66] B. Song, C. Galasso, Directivity-induced pulse-like ground motions and fracture risk of pre-northridge welded column splices, J. Earthq. Eng. (2020) 1–19, https://doi.org/10.1080/13632469.2020.1772154.
[67] V. Silva, D. Amo-Oduro, A. Calderon, C. Costa, J. Dabbeek, V. Despotaki, L. Martins, M. Pagani, A. Rao, M. Simionato, D. Viganò, C. Yepes-Estrada, A. Acevedo, H. Crowley, N. Horspool, K. Jaiswal, M. Journeay, M. Pittore, Development of a global seismic risk model, Earthq. Spectra 36 (2020) 372–394, https://doi.org/10.1177/8755293019899953.